

Implementation of Measurement Reduction for the Variational Quantum Eigensolver

Alexis Ralli,^{1,*} Peter J. Love,^{2,3,†} Andrew Tranter,^{2,‡} and Peter V. Coveney^{1,4,§}

¹Centre for Computational Science, Department of Chemistry, University College London, WC1H 0AJ, UK

²Department of Physics and Astronomy, Tufts University, Medford, MA 02155, USA

³Computational Science Initiative, Brookhaven National Laboratory, Upton, NY 11973, USA

⁴Informatics Institute, University of Amsterdam, Amsterdam, 1098 XH, Netherland

(Dated: September 30, 2021)

One limitation of the variational quantum eigensolver algorithm is the large number of measurement steps required to estimate different terms in the Hamiltonian of interest. Unitary partitioning reduces this overhead by transforming the problem Hamiltonian into one containing fewer terms. We explore two different circuit constructions of the transformation required - one built by a sequence of rotations and the other a linear combination of unitaries (LCU). To assess performance, we simulated chemical Hamiltonians and studied the ground states of H₂ and LiH. Both implementations are successful even in the presence of noise. The sequence of rotations realization offers the greatest benefit, whereas the probabilistic nature of LCU reduces its effectiveness. To our knowledge, this work also demonstrates the first experimental implementation of LCU on quantum hardware.

Introduction.— Current quantum computing devices have significant limitations, namely short coherence times, low qubit numbers and little to no error correction. These machines are termed noisy intermediate-scale quantum (NISQ) computers [1]. The leading candidate algorithms for use on NISQ devices are variational hybrid quantum-classical algorithms such as the variational quantum eigensolver (VQE) and quantum approximate optimization algorithm (QAOA) [2, 3]. VQE estimates Hamiltonian eigenvalues on near term quantum computers [3]. Many different implementations of the algorithm have been performed utilizing a wide array of different quantum platforms [4–7].

VQE has been widely applied to the electronic structure problem. The second quantized form of the molecular electronic Hamiltonian is converted to a qubit Hamiltonian by the Jordan-Wigner, Bravyi-Kitaev or related transformations [8–10]. The resulting qubit Hamiltonian is a linear combination of m Pauli operators on n qubits:

$$H_q = \sum_{i=0}^{m-1} c_i P_i = \sum_{i=0}^{m-1} c_i \left(\sigma_0^i \otimes \sigma_1^i \otimes \dots \otimes \sigma_{n-1}^i \right), \quad (1)$$

where c_i are real coefficients, P_i are n -qubit Pauli operators, which are n -fold tensor products of 1-qubit Pauli operators, or the 2×2 identity matrix: $\sigma_j^i \in \{X, Y, Z, \mathcal{I}\} \forall i$, and j indexes the qubit the operator acts on.

In general, the number of terms in equation (1) scales as $\mathcal{O}(N_o^4)$, where N_o is the number of orbitals [11]. The linearity of expectation values allows

$$E(\vec{\theta}) = \langle H_q \rangle = \sum_{i=0}^{m-1} c_i \langle \psi(\vec{\theta}) | P_i | \psi(\vec{\theta}) \rangle, \quad (2)$$

where $|\psi(\vec{\theta})\rangle$ is an ansatz state produced by a parameterized quantum circuit. In conventional VQE, the expectation value of each subterm $\langle P_i \rangle$ is determined independently.

An estimate of each term's expectation value $\langle P_i \rangle$ is found by averaging over M_i repeated measurement outcomes $\{s_j^{(i)}\}_{j=1,2,\dots,M_i}$ via [3, 12, 13]:

$$\langle P_i \rangle = c_i \langle \psi(\vec{\theta}) | P_i | \psi(\vec{\theta}) \rangle \approx c_i \left(\frac{1}{M_i} \sum_{j=1}^{M_i} s_j^{(i)} \right), \quad (3)$$

where $s_j^{(i)} \in \{-1, +1\}$. The above expression is exact as the number of samples $M_i \rightarrow \infty$.

A finite number of runs is used to estimate each $\langle P_i \rangle$ term and thus each outcome will belong to a distribution centred around the expectation value $\langle \psi(\vec{\theta}) | P_i | \psi(\vec{\theta}) \rangle$ with standard deviation ϵ_i . Each estimate $\langle \psi(\vec{\theta}) | P_i | \psi(\vec{\theta}) \rangle$ is derived from sums of random variables with finite variance. Due to the central limit theorem, they must converge to a normal distribution [12]. Because we will be comparing Hamiltonians with different numbers of terms, we will take a slightly different approach. We combine a single sample of all terms into a single-shot energy estimate $e_j = \sum_i c_i s_j^{(i)}$. The distribution of this estimate determines how many samples are required to achieve a given error on the mean. We do not assume normality but instead use bootstrapping to obtain confidence intervals.

The optimal number of repetitions M_i to achieve a certain precision ϵ is [14, 15]:

$$N = \sum_{i=0}^{m-1} M_i = \frac{1}{\epsilon^2} \left(\sum_{i=0}^{m-1} |c_i| P_i \right)^2 \leq \frac{1}{\epsilon^2} \left(\sum_{i=0}^{m-1} |c_i| \right)^2, \quad (4)$$

where N is the total number of samples. Since the number of terms in equation 1 scales as $\mathcal{O}(N_o^4)$, the total number of measurements required will scale as $\mathcal{O}(N_o^6/\epsilon^2)$, where chemical accuracy is defined as $\epsilon = 1$ kcal/mol (1.6 mHa), the accuracy required to match typical thermochemical experiments. Wecker *et al.* showed that to obtain energy estimates for HeH⁺, BeH₂ and H₂O requires

$10^8 - 10^9$ samples to achieve an error of 1 *mHa* [14]. This implies that the number of measurements required is an obstacle for experimental implementations of VQE to the number of qubits currently available on NISQ devices.

For example, take the experimental implementation of VQE by Hempel *et al.*, which took 20 *ms* to perform each VQE repetition on a trapped ion quantum computer [6]. To obtain the ground state energy of H_2 , in a minimal basis to within chemical accuracy, of order 14000 repetitions were needed and 4.6 minutes of averaging required. Recently, the largest implementation of VQE to date was only able to make use of 12 qubits out of 53 available [7].

Various approaches have been proposed for reducing the total number of samples required by VQE [16–24]. In this paper, we focus on the unitary partitioning procedure independently proposed by Verteletskyi *et al.* [25] and Zhao *et al.* [26]. The main idea of this approach is to partition the qubit Hamiltonian into groups of n -fold Pauli operators whose linear combination is unitary. The overall operator represented by these sums can then be measured at once using additional coherent resources. In this work, we compare two different circuit realizations of unitary partitioning, as proposed in [26].

Unitary partitioning.— The operators P_i are Hermitian and unitary, however, a sum of unitary operators is in general non-unitary. In order to make $\sum_j c_j P_j$ unitary three constraints are imposed [25, 26]: (1) $\{P_i, P_j\} = 2\delta_{i,j}$, (2) $\sum_j |c_j|^2 = 1$ and (3) $\text{Im}(c_j^* c_i) = 0$. Here $\{.,.\}$ is the anticommutator ($\{A, B\} \equiv AB + BA$). The first condition is satisfied by partitioning the qubit Hamiltonian H_q into m_c sets denoted $\{S_l\}_{l=0,2,\dots,m_c-1}$. The sub-Hamiltonian corresponding to each anticommuting set H_{S_l} is defined as:

$$H_{S_l} = \sum_{\substack{j=0 \\ P_j \in S_l}}^{|S_l|-1} c_j^{(l)} P_j^{(l)}. \quad (5)$$

S_l is the set of P_i terms in H_{S_l} , where $\{P_j, P_i\} = 0 \forall P_j \neq P_i \in S_l$. The process of finding such sets is discussed in [22, 25, 26] and formulated as a minimum clique cover problem. This is an NP-hard problem [27]; however, heuristic algorithms can provide sufficiently good approximate solutions to this problem [17, 25, 28]. Condition (2) is satisfied by re-normalising each anticommuting set:

$$H_{S_l} = \gamma_l \sum_{\substack{j=0 \\ P_j \in S_l}}^{|S_l|-1} \beta_j^{(l)} P_j^{(l)}, \quad (6)$$

where $\sum_j (\beta_j^{(l)})^2 = 1$ and $c_j^{(l)} = \gamma_l \beta_j^{(l)}$. The final condition is already satisfied, as all the coefficients c_i in H_q are real.

Using the unitary partitioning method, the qubit

Hamiltonian is separated into m_c sets of unitary sums:

$$H_q = \sum_{i=0}^{m-1} c_i P_i = \sum_{l=0}^{m_c-1} H_{S_l} = \sum_{l=0}^{m_c-1} \gamma_l \sum_{\substack{j=0 \\ P_j \in S_l}}^{|S_l|-1} \beta_j^{(l)} P_j^{(l)}. \quad (7)$$

Each sum $\sum_{P_j \in S_l} \beta_j^{(l)} P_j^{(l)}$ can be written as $R_l^\dagger Q_l R_l$, due to the spectral decomposition property of Hermitian operators. The expectation value of the Hamiltonian can therefore be obtained via:

$$\langle \psi | H_q | \psi \rangle = \sum_{l=0}^{m_c-1} \gamma_l \langle \psi | R_l^\dagger Q_l R_l | \psi \rangle, \quad (8)$$

and only $m_c \leq m$ terms are estimated, at the expense of needing to implement R_l coherently within each circuit [26]. We explore two different approaches to construct R_l - one an ordered sequence of rotations [26] and the other based on a linear combination of unitaries (LCU) [29]. These methods follow the constructions outlined in [26] and are fully described in the Supplemental Material. Fig. 1 shows the general circuit structure of each approach, note that Q_l in these circuits is represented by the n -fold Pauli operator $P_k^{(l)}$.

In this work, the operator R_l required by unitary partitioning is implemented by either a sequence of rotations or LCU. The LCU technique uses ancilla qubits to implement a single rotation around an axis defined by the elements of the anticommuting set [26, 29]. The LCU technique is more complex than the sequence of rotations. To reduce the overheads required, we considered different circuit optimizations and these are given in the Supplemental Material.

Results.— We consider Hamiltonians for H_2 and LiH molecules employing the STO-3G and STO-6G basis sets respectively. These were calculated using Openfermion-PySCF and converted into the qubit Hamiltonian using the Bravyi-Kitaev transformation in OpenFermion [30, 31]. Partitioning into anticommuting sets H_{S_l} was performed using networkX [32]. Further details are given in the Supplemental Material. In all cases the exact ground state was used as the input state $|\psi(\vec{\theta})\rangle$. We avoided ansatz optimization because our aim is to investigate the implementation of unitary partitioning.

For a given preparation of the true ground state of H_2 , we compare both implementations of measurement reduction by unitary partitioning against a standard VQE calculation on IBM's open access quantum device (ibmq 5 Yorktown - ibmqx2) and Qiskit's qasm simulator [33]. The quantum circuits required are given in the Supplemental Material. Fig. 2 shows the distribution of single-shot energy estimates - $e_j = \sum_i c_i s_j^{(i)}$ - of all three techniques applied to molecular hydrogen. The average energy is given by $\langle E \rangle = \frac{1}{N} \sum_{j=0}^{N-1} e_j$. To compare each method the total number of calls to the quantum computer for each technique was fixed at $N = 1266300$. A

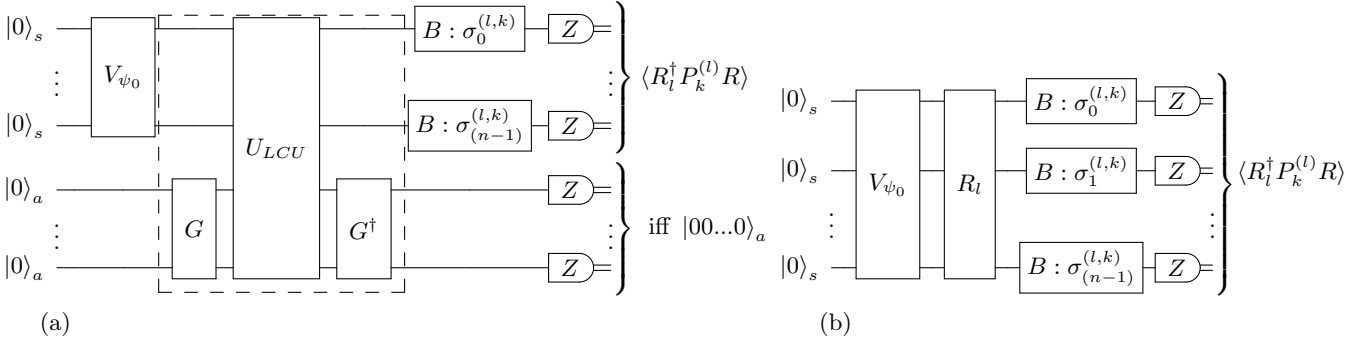


FIG. 1: General quantum circuit implementations of unitary partitioning constructed as (a) a LCU and (b) a sequence of rotations. The subscripts s and a denote system and ancilla registers respectively. V_{ψ_0} is a unitary gate that prepares the ground state. To measure the qubits in the computational basis, the single qubit gates $B \in \{H, R_x(-\pi/2), \mathcal{I}\}$ are required to perform a change of basis dependent on the Pauli operator measured. G and U_{LCU} encode the R_l operator as $\langle 00\dots 0 |_a G^\dagger U_{LCU} G | 00\dots 0 \rangle_a = R_l / \|\alpha^{(l)}\|_1$ and are defined in the Supplemental Material. Note $\|\alpha^{(l)}\|_1$ is the l_1 norm of R_l .

calibration matrix method available in qiskit was used to mitigate measurement errors and was used to amend the raw outputs from ibmqx2.

The qubit Hamiltonian for H_2 has five terms, which is reduced to three by unitary partitioning, not including the identity term. The number of energy estimates e_j obtained was 253260 for standard VQE and 5/3 this for unitary partitioning by the sequence of rotations method. This is because the smaller number of terms allowed a correspondingly larger number of samples to be taken for a fixed N . The total number of e_j samples from ibmqx2 for these techniques was reduced to 253074 and 421951 after measurement error mitigation was applied. The LCU approach to unitary partitioning is probabilistic and requires post-selection on the all zero state of the ancilla register. After post-selection, our simulation of unitary partitioning as a LCU on ibmqx2 gave 333407 raw e_j samples and 332763 e_j samples after measurement error mitigation was applied to the raw output. Our emulation of this method on a noise-free quantum processing unit (QPU) gave 336390 e_j samples after post-selection. The theoretical maximum possible number of samples for LCU would be the same as the sequence of rotations method if all samples obtained were successful.

The reason a normal distribution is not obtained is due to the number of terms in the qubit Hamiltonian for H_2 . At most only 32 distinct values of e_j are possible for standard VQE and 8 under unitary partitioning, and so we do not expect the central limit argument to apply here.

To investigate the distribution of energies obtained from each method in more detail, we simulated the larger problem of LiH using Qiskit's statevector simulator [33]. Further details are given in the Supplemental Material, Fig. 3 summarizes the results. Again, each data point is an energy estimate found from the weighted measure-

ment outcomes of a single-shot VQE run. The standard qubit Hamiltonian for this problem is made up of 630 terms and after applying unitary partitioning 102 terms, not including the identity term. The total number of circuit samples for each technique was fixed at $N = 1018521000$. The total number of energy estimates e_j for standard VQE, the sequence of rotations and the LCU methods after post-selection were 1616700, 9985500 and 1447349 respectively.

We performed the Kolmogorov-Smirnov [34] and Shapiro-Wilk tests [35] on the data in Fig. 3 to check for normality. The P-values obtained in all cases were smaller than 0.05, and thus we could not assume a normal distribution. This may be caused by insufficient samples allowing convergence to the central limit or the problem size still being too small. To estimate the statistics of the true distribution we thus employed bootstrap resampling [36].

Discussion.— To benchmark each method we compare the standard deviation (σ) and standard error of the mean (SEM) of the ground state energies calculated. The SEM describes how precise the mean of the sample is as an estimate of the true population mean and is defined as $SEM = \sigma/\sqrt{N}$, where N is the total number of samples. 95% confidence intervals (CI) were calculated using bootstrapping with 10,000 resamples with replacement. The full statistical analysis is given in Table IV in the Supplemental Material.

Qualitatively, the noise-free LiH simulation results in Fig. 3 show that VQE with unitary partitioning applied as either a LCU or a sequence of rotations give a similar distribution of energies compared to standard VQE.

Quantitatively, the σ of ground state energy estimates of LiH for each method were very similar, with the largest difference being 4.8 mHa . Whereas for the noise-free simulation of H_2 (Fig. 2c), the standard deviation of

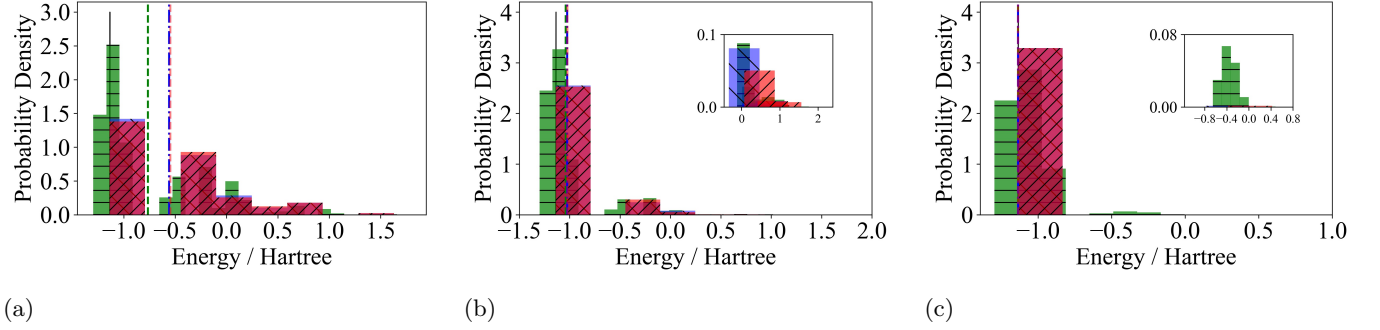


FIG. 2: Probability density functions of single-shot VQE estimates of the ground state energy e_j of H_2 . A bin is given to every possible energy outcome. The green horizontal dashed bars show data from standard VQE. The red forward slashed and blue backslashed bars are results from VQE with unitary partitioning applied as a LCU and a sequence of rotations respectively. The dashed vertical lines show the average energy for each method and the solid black vertical interval represents chemical accuracy ($E_{FCI} = -1.13728 Ha$). The raw results from ibmqx2 are given in (a), (b) shows these results with measurement error mitigation applied and (c) gives results from simulation on a noise-free QPU.

e_j from VQE with unitary partitioning applied were an order of magnitude lower than standard VQE. We expect this is due to the small number of distinct e_j outcomes for this problem under unitary partitioning. Note σ gives a measure of how spread the single-shot ground state energy estimates are from the mean and is independent of the number of samples N taken.

The SEM then takes into account the total number of samples. As unitary partitioning is designed to require fewer terms to be measured, for a fixed number of calls N to a QPU, the total number of energy estimates will be larger. The sequence of rotations construction of unitary partitioning is deterministic and will always give more e_j samples than conventional VQE. Hence, the SEM of both H_2 and LiH noiseless simulations using the sequence of rotations method were an order of magnitude lower than standard VQE. On the other hand, the LCU realization of unitary partitioning is probabilistic. Even though fewer terms need measurement, post-selection requires some samples to be discarded. We see this in the simulation for LiH, where the LCU approach actually has the fewest e_j samples at 1447349 compared to 1616700 for standard VQE. As the σ of all three approaches are similar, the LCU implementation has the highest SEM in this case. The advantage over standard VQE is thus dependent on the success probability, which for each circuit is given by the inverse l_1 norm squared of the operator to be implemented as a LCU. Importantly post-selection is only performed on the ancilla register. The success probability is inversely proportional to the dimension of the ancilla Hilbert space. The number of ancilla qubits scales logarithmically with the number of terms in each anticommuting set ($n_{ancilla} = \lceil \log_2(|H_{S_l}| - 1) \rceil$), and the dimension of the ancilla Hilbert space, and hence success probability, is inversely proportional to the size of the anticommuting sets.

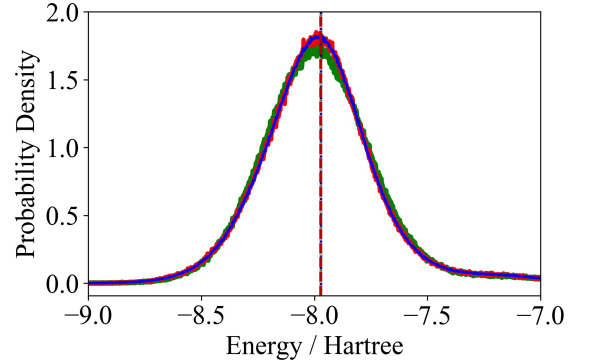


FIG. 3: Probability density function of single-shot VQE estimates of the ground state energy e_j of LiH, from a noise-free QPU simulation. The number of bins was set to 2500 and the centre of each was plotted. The green line shows data from standard VQE. The red and blue lines are results from VQE with unitary partitioning applied as a LCU and a sequence of rotations respectively. The dashed vertical lines show the average energy for each method and the solid black vertical line shows the FCI ground state energy ($-7.97118 Ha$). Individual plots are given in the Supplemental Material.

The experimental results for H_2 on ibmqx2 show that applying the unitary partitioning technique does not appreciably change the performance of VQE, when combined with error mitigation techniques. We suspect this is due to the extra coherent resource required to perform R_l causing an increase in errors, which offsets the improvement of the SEM given by the technique. We expect this to be mitigated as gate fidelities increase.

The experimental execution of R_l by LCU on ibmqx2 performed comparably to the sequence of rotations re-

alization. Ignoring post-selection issues, the LCU algorithm is more complex and requires more qubits to implement. We believe this motivates further examination of the use of more advanced quantum algorithms on NISQ devices.

A particular feature of our results from ibmqx2 (Fig. 2) is that the mean ground state energy obtained is overestimated by a seemingly constant amount. We suspect this could be due to two effects. Firstly, our ansatz circuit prepares the ground state. Any coherent errors in this circuit will increase the energy of the state prepared by virtue of the variational principle [37]. Secondly, inspecting the qubit Hamiltonian for H_2 most coefficients are positive. As our results overestimate the energy, it implies that measurement outcomes of each n -fold Pauli operator are more frequently $+1$ causing each estimate of e_j to be larger. This could be an indication of a higher $|0\rangle$ count on each qubit or $P(0|1) > P(1|0)$.

The single-qubit gate error rates of IBM QPU's have error rates in the range of 0.1%-0.3% and two-qubit gate errors in the range of 2%-5% [38]. The most error-prone operation is measurement and ibmqx2 on average has a measurement error rate of 4%, but this can be much higher (13%) [38]. This large measurement error is apparent when comparing the raw and measurement error mitigated results from the QPU simulation of H_2 . In future experiments, it would be interesting to improve measurement fidelity, for example by using invert-and-measure designs [38] as well as flipping the qubit encoding ($|0\rangle \mapsto |1\rangle$ and $|1\rangle \mapsto |0\rangle$) as in [39], or by other mitigation schemes [40].

In the original work in which these techniques were proposed, it was shown that the variance of the different methods should be similar [26]. This is observed on both the QPU emulator and quantum device.

Crucially, when partitioning the qubit Hamiltonian into anticommuting cliques (equation 7), the greatest measurement reduction is obtained if the minimum clique cover is found. This cover has the fewest H_{S_l} sets possible. However, non-optimal clique covers still give a measurement reduction. As the size of the quantum circuit for R_l is proportional to the number of terms in H_{S_l} , we propose that for practical applications a non-optimal clique cover is beneficial. By splitting the problem Hamiltonian into pairs of anticommuting operators ($|H_{S_l}| = 2 \forall \{l\}_{l=0,1,\dots,m_c-1}$), the extra coherent resources required to perform R_l are experimentally realistic for current and near term devices. This offers a constant factor improvement to the number of measurements required. A detailed circuit depth analysis for each realization is given in the Supplemental Material.

Conclusion.— Our work shows that the unitary partitioning technique for measurement reduction can significantly improve the precision of variational calculations. For a fixed number of calls N to the quantum computer, fewer terms need to be estimated and thus the total num-

ber of separate energy estimates is increased. As the standard deviation of energies is similar for the different approaches, the standard error of the mean will be lower when unitary partitioning is applied. Our results indicate the deterministic sequence of rotations implementation offers the best improvement, which we find in our noiseless simulation of H_2 and LiH . In contrast, the LCU approach is probabilistic and some measurements must be discarded. The advantage over standard VQE is thus dependent on the success probability. This naive implementation of LCU can be improved by using oblivious and standard amplitude amplification [41–43], which can boost the probability of success. However, further coherent resources are required.

The experimental results obtained using IBM's NISQ device (ibmqx2) show unitary partitioning changed the performance of VQE negligibly for a fixed N . Even though unitary partitioning requires fewer terms to be combined to give an energy estimate leading to less statistical noise and more energy samples, we suspect the additional coherent resources required causes an increased error accumulation, which offsets the advantages given by the technique. As quantum devices continue to improve, this effect should be reduced.

Our work shows how precision can be improved for a fixed number of calls to a QPU; however, an alternate outlook is how this technique may allow larger problems to be studied. For a given precision, applying unitary partitioning requires fewer samples and thus may allow larger scale simulations to be performed on reasonable timescales.

Future work will investigate how the variance of energies obtained changes if different terms in H_{S_l} are reduced to, as there is flexibility in the unitary partitioning technique. We also note that this work has an interesting application to the recently proposed frugal shot Rosalin optimizer [44], which uses a weighted random sampling of Hamiltonian terms. Unitary partitioning transforms the Hamiltonian of interest into one with fewer terms of different coefficients; the effect this has on the optimizer's performance is an interesting avenue to explore.

Acknowledgments.— A. R. acknowledges support from the Engineering and Physical Sciences Research Council (EP/L015242/1). P. J. L. and A. T. acknowledge support by the NSF STAQ project (PHY-1818914). P. V. C. is grateful for funding from the European Commission for VECMA (800925). A. R. would also like to thank J. Dborin for useful discussions.

* alexis.ralli.18@ucl.ac.uk

† peter.love@tufts.edu

‡ tufts@atranter.net

§ p.v.coveney@ucl.ac.uk

- [1] J. Preskill, Quantum computing in the NISQ era and beyond, *Quantum* **2**, 79 (2018).
- [2] E. Farhi, J. Goldstone, and S. Gutmann, A quantum approximate optimization algorithm, arXiv preprint arXiv:1411.4028 (2014).
- [3] A. Peruzzo, J. McClean, P. Shadbolt, M.-H. Yung, X.-Q. Zhou, P. J. Love, A. Aspuru-Guzik, and J. L. O’Brien, A variational eigenvalue solver on a photonic quantum processor, *Nature Communications* **5**, 4213 (2014).
- [4] J. I. Colless, V. V. Ramasesh, D. Dahlen, M. S. Blok, M. Kimchi-Schwartz, J. McClean, J. Carter, W. De Jong, and I. Siddiqi, Computation of molecular spectra on a quantum processor with an error-resilient algorithm, *Physical Review X* **8**, 011021 (2018).
- [5] A. A. Gentile, R. Santagati, J. Wang, S. Paesani, N. Wiebe, J. McClean, D. Bonneau, J. W. Silverstone, S. Morley-Short, P. J. Shadbolt, D. P. Tew, X. Zhou, J. L. O’Brien, and M. G. Thompson, Exploring network structure, dynamics, and function using networkx, in *2018 Conference on Lasers and Electro-Optics Pacific Rim (CLEO-PR)* (2018) pp. 1 – 2.
- [6] C. Hempel, C. Maier, J. Romero, J. McClean, T. Monz, H. Shen, P. Jurcevic, B. P. Lanyon, P. Love, R. Babbush, *et al.*, Quantum chemistry calculations on a trapped-ion quantum simulator, *Physical Review X* **8**, 031022 (2018).
- [7] G. A. Quantum *et al.*, Hartree-fock on a superconducting qubit quantum computer, *Science* **369**, 1084 (2020).
- [8] J. T. Seeley, M. J. Richard, and P. J. Love, The Bravyi-Kitaev transformation for quantum computation of electronic structure, *The Journal of Chemical Physics* **137**, 224109 (2012).
- [9] S. B. Bravyi and A. Y. Kitaev, Fermionic quantum computation, *Annals of Physics* **298**, 210 (2002).
- [10] P. Jordan and E. P. Wigner, Über das paulische äquivalenzverbot, in *The Collected Works of Eugene Paul Wigner* (Springer, 1993) pp. 109–129.
- [11] Y. Cao, J. Romero, J. P. Olson, M. Degroote, P. D. Johnson, M. Kieferová, I. D. Kivlichan, T. Menke, B. Peropadre, N. P. Sawaya, *et al.*, Quantum chemistry in the age of quantum computing, *Chemical Reviews* **119**, 10856 (2019).
- [12] J. R. McClean, J. Romero, R. Babbush, and A. Aspuru-Guzik, The theory of variational hybrid quantum-classical algorithms, *New Journal of Physics* **18**, 023023 (2016).
- [13] G. G. Guerreschi and M. Smelyanskiy, Practical optimization for hybrid quantum-classical algorithms, arXiv preprint arXiv:1701.01450 (2017).
- [14] D. Wecker, M. B. Hastings, and M. Troyer, Progress towards practical quantum variational algorithms, *Physical Review A* **92**, 042303 (2015).
- [15] N. C. Rubin, R. Babbush, and J. McClean, Application of fermionic marginal constraints to hybrid quantum algorithms, *New Journal of Physics* **20**, 053020 (2018).
- [16] A. Kandala, A. Mezzacapo, K. Temme, M. Takita, M. Brink, J. M. Chow, and J. M. Gambetta, Hardware-efficient variational quantum eigensolver for small molecules and quantum magnets, *Nature* **549**, 242 (2017).
- [17] V. Verteletskyi, T.-C. Yen, and A. F. Izmaylov, Measurement optimization in the variational quantum eigensolver using a minimum clique cover, *The Journal of Chemical Physics* **152**, 124114 (2020).
- [18] A. F. Izmaylov, T.-C. Yen, and I. G. Ryabinkin, Revising the measurement process in the variational quantum eigensolver: is it possible to reduce the number of separately measured operators?, *Chemical Science* **10**, 3746 (2019).
- [19] J. Cotler and F. Wilczek, Quantum overlapping tomography, *Physical Review Letters* **124**, 100401 (2020).
- [20] X. Bonet-Monroig, R. Babbush, and T. E. O’Brien, Nearly optimal measurement scheduling for partial tomography of quantum states, arXiv preprint arXiv:1908.05628 (2019).
- [21] P. Gokhale and F. T. Chong, $o(n^3)$ measurement cost for variational quantum eigensolver on molecular hamiltonians, arXiv preprint arXiv:1908.11857 (2019).
- [22] A. Jena, S. Genin, and M. Mosca, Pauli partitioning with respect to gate sets, arXiv preprint arXiv:1907.07859 (2019).
- [23] W. J. Huggins, J. McClean, N. Rubin, Z. Jiang, N. Wiebe, K. B. Whaley, and R. Babbush, Efficient and noise resilient measurements for quantum chemistry on near-term quantum computers, arXiv preprint arXiv:1907.13117 (2019).
- [24] P. Gokhale, O. Angiuli, Y. Ding, K. Gui, T. Tomesh, M. Suchara, M. Martonosi, and F. T. Chong, Minimizing state preparations in variational quantum eigensolver by partitioning into commuting families, arXiv preprint arXiv:1907.13623 (2019).
- [25] A. F. Izmaylov, T.-C. Yen, R. A. Lang, and V. Verteletskyi, Unitary partitioning approach to the measurement problem in the variational quantum eigensolver method, *Journal of Chemical Theory and Computation* **16**, 190 (2020).
- [26] A. Zhao, A. Tranter, W. M. Kirby, S. F. Ung, A. Miyake, and P. J. Love, Measurement reduction in variational quantum algorithms, *Physical Review A* **101**, 062322 (2020).
- [27] R. M. Karp, *Complexity of Computer Computations* (Springer, 1972) pp. 85–103.
- [28] A. Tranter, P. J. Love, F. Mintert, N. Wiebe, and P. V. Coveney, Ordering of trotterization: Impact on errors in quantum simulation of electronic structure, *Entropy* **21**, 1218 (2019).
- [29] A. M. Childs and N. Wiebe, Hamiltonian simulation using linear combinations of unitary operations, *Quantum Info. Comput.* **12**, 901 (2012).
- [30] J. McClean, N. Rubin, K. Sung, I. D. Kivlichan, X. Bonet-Monroig, Y. Cao, C. Dai, E. S. Fried, C. Gidney, B. Gimby, *et al.*, Openfermion: the electronic structure package for quantum computers, *Quantum Science and Technology* (2020).
- [31] Q. Sun, T. C. Berkelbach, N. S. Blunt, G. H. Booth, S. Guo, Z. Li, J. Liu, J. D. McClain, E. R. Sayfutyarova, S. Sharma, *et al.*, Pyscf: the python-based simulations of chemistry framework, *Wiley Interdisciplinary Reviews: Computational Molecular Science* **8**, e1340 (2018).
- [32] A. A. Hagberg, D. A. Schult, and P. J. Swart, Exploring network structure, dynamics, and function using networkx, in *Proceedings of the 7th Python in Science Conference*, edited by G. Varoquaux, T. Vaught, and J. Millman (Pasadena, CA USA, 2008) pp. 11 – 15.
- [33] H. Abraham, AduOftei, R. Agarwal, I. Y. Akhalwaya, G. Aleksandrowicz, T. Alexander, M. Amy, E. Arbel, *et al.*, Qiskit: An open-source framework for quantum computing (2019).

- [34] F. J. Massey Jr, The kolmogorov-smirnov test for goodness of fit, *Journal of the American Statistical Association* **46**, 68 (1951).
- [35] S. S. Shapiro and M. B. Wilk, An analysis of variance test for normality (complete samples), *Biometrika* **52**, 591 (1965).
- [36] B. Efron, Bootstrap methods: Another look at the jack-knife, in *Breakthroughs in Statistics* (Springer, 1992) pp. 569–593.
- [37] A. Szabo and N. S. Ostlund, *Modern Quantum Chemistry: Introduction to Advanced Electronic Structure Theory*, 1st ed. (Dover Publications Inc., New York, 2012).
- [38] S. S. Tannu and M. K. Qureshi, Mitigating measurement errors in quantum computers by exploiting state-dependent bias, in *Proceedings of the 52nd Annual IEEE/ACM International Symposium on Microarchitecture* (2019) pp. 279–290.
- [39] Y. Nam, J.-S. Chen, N. C. Pienti, K. Wright, C. Delaney, D. Maslov, K. R. Brown, S. Allen, J. M. Amini, J. Apisdorf, *et al.*, Ground-state energy estimation of the water molecule on a trapped-ion quantum computer, *npj Quantum Information* **6**, 1 (2020).
- [40] Y. Chen, M. Farahzad, S. Yoo, and T. C. Wei, Detector tomography on ibm quantum computers and mitigation of an imperfect measurement, *Physical Review A* **100**, 052315 (2019).
- [41] D. W. Berry, A. M. Childs, R. Cleve, R. Kothari, and R. D. Somma, Exponential improvement in precision for simulating sparse hamiltonians, in *Proceedings of the 46th Annual ACM Symposium on Theory of Computing* (Association for Computing Machinery, 2014) pp. 283–292.
- [42] L. K. Grover, Quantum mechanics helps in searching for a needle in a haystack, *Physical Review Letters* **79**, 325 (1997).
- [43] M. Boyer, G. Brassard, P. Hoyer, and A. Tapp, Tight bounds on quantum searching, *Fortschritte der Physik: Progress of Physics* **46**, 493 (1998).
- [44] A. Arrasmith, L. Cincio, R. D. Somma, and P. J. Coles, Operator sampling for shot-frugal optimization in variational algorithms, *arXiv preprint arXiv:2004.06252* (2020).
- [45] G. H. Low and I. L. Chuang, Hamiltonian Simulation by Qubitization, *Quantum* **3**, 163 (2019).
- [46] S. Subramanian, S. Brierley, and R. Jozsa, Implementing smooth functions of a hermitian matrix on a quantum computer, *Journal of Physics Communications* **3**, 065002 (2019).
- [47] J. D. Whitfield, J. Biamonte, and A. Aspuru-Guzik, Simulation of electronic structure hamiltonians using quantum computers, *Molecular Physics* **109**, 735 (2011).
- [48] G.-L. Long and Y. Sun, Efficient scheme for initializing a quantum register with an arbitrary superposed state, *Physical Review A* **64**, 014303 (2001).
- [49] M. A. Nielsen and I. Chuang, *Quantum computation and quantum information: 10th anniversary edition* (Cambridge University Press, 2002) 10th ed., Chap. 4, p. 184.
- [50] M. Z. Rahman and J. E. Rice, Templates for positive and negative control toffoli networks, in *International Conference on Reversible Computation* (Springer, 2014) pp. 125–136.
- [51] R. Babbush, C. Gidney, D. W. Berry, N. Wiebe, J. McClean, A. Paler, A. Fowler, and H. Neven, Encoding electronic spectra in quantum circuits with linear t complexity, *Physical Review X* **8**, 041015 (2018).
- [52] G. Frank, Pulse code communication (1953), uS Patent 2,632,058.
- [53] Y. Nam, N. J. Ross, Y. Su, A. M. Childs, and D. Maslov, Automated optimization of large quantum circuits with continuous parameters, *npj Quantum Information* **4**, 1 (2018).
- [54] P. J. O’Malley, R. Babbush, I. D. Kivlichan, J. Romero, J. R. McClean, R. Barends, J. Kelly, P. Roushan, A. Tranter, N. Ding, *et al.*, Scalable quantum simulation of molecular energies, *Physical Review X* **6**, 031007 (2016).
- [55] F. Leymann and J. Barzen, The bitter truth about gate-based quantum algorithms in the NISQ era, *Quantum Science and Technology* **5**, 044007 (2020).

Implementation of Measurement Reduction for the Variational Quantum Eigensolver - Supplemental Material

Alexis Ralli,^{1,*} Peter J. Love,^{2,3,†} Andrew Tranter,^{2,‡} and Peter V. Coveney^{1,4,§}

¹*Centre for Computational Science, Department of Chemistry, University College London, WC1H 0AJ, UK*

²*Department of Physics and Astronomy, Tufts University, Medford, MA 02155, USA*

³*Computational Science Initiative, Brookhaven National Laboratory, Upton, NY 11973, USA*

⁴*Informatics Institute, University of Amsterdam, Amsterdam, 1098 XH, Netherland*

(Dated: September 30, 2021)

CONTENTS

Acknowledgments	5
References	5
I. Unitary partitioning - construction of R_l	9
A. Ordered sequence of rotations procedure	9
B. Linear combination of unitaries method	10
1. LCU technique overview	10
2. Toy LCU example	12
3. LCU approach to unitary partitioning	13
II. Circuit depth analysis	15
A. Sequence of rotations implementation	15
B. LCU implementation	16
1. LCU cascade	17
2. LCU direct	18
3. LCU constant factor ($ H_{S_l} \leq 5$)	19
4. Further LCU simplifications	19
III. Numerical study	19
A. Molecular Hydrogen	20
1. Sequence of rotations quantum circuits	21
2. LCU quantum circuits	22
3. Standard VQE quantum circuits	24
4. Measurement error mitigation	25
B. Lithium Hydride	26
C. Statistical analysis	26
D. LiH histogram results	27

I. UNITARY PARTITIONING - CONSTRUCTION OF R_l

The unitary partitioning method uses the property that the expectation value of any Hermitian qubit operator can be obtained via a single set of single-qubit measurements, because it can be written in terms of its spectral decomposition. For example, consider the Hermitian operator $A = \sum_{a=0}^{d-1} \lambda_a |\psi_a\rangle \langle \psi_a|$, d is the dimension of the space and A acts on orthonormal states $|\psi_a\rangle$. Each $|\psi_a\rangle$ is an eigenstate of the operator with corresponding eigenvalue λ_a . As the set of eigenvectors $\{|\psi_a\rangle\}$ form an orthonormal basis there always exists a unitary R that maps this basis to another: $R|\psi_a\rangle = |e_a\rangle$ or $|\psi_a\rangle = R^\dagger |e_a\rangle$. The operator A can be written in this basis: $A = \sum_{a=1}^d \lambda_a R^\dagger |e_a\rangle \langle e_a| R = R^\dagger \left(\sum_{a=1}^d \lambda_a |e_a\rangle \langle e_a| \right) R = R^\dagger Q R$. The expectation value of A can be found by $\langle A \rangle = \langle \psi | A | \psi \rangle = \langle \psi | R^\dagger Q R | \psi \rangle$. This idea underpins the unitary partitioning method.

As discussed in the main text, the unitary partitioning technique splits the Hamiltonian into m_c sets of unitary sums:

$$H_q = \sum_{i=0}^{m-1} c_i P_i = \sum_{l=0}^{m_c-1} H_{S_l} = \sum_{l=0}^{m_c-1} \gamma_l \sum_{\substack{j=0 \\ P_j \in S_l}}^{|H_{S_l}|-1} \beta_j^{(l)} P_j^{(l)}, \quad (9)$$

where H_{S_l} represents an anticommuting set defined as:

$$H_{S_l} = \sum_{\substack{j=0 \\ P_j \in S_l}}^{|H_{S_l}|-1} c_j^{(l)} P_j^{(l)}. \quad (10)$$

S_l is the set of P_i terms in H_{S_l} , where $\{P_j, P_i\} = 0 \ \forall P_j \neq P_i \in S_l$. The operator represented by each sum $\sum_{P_j \in S_l} \beta_j^{(l)} P_j^{(l)}$ is a unitary Hermitian operator and can thus be written as $R_l^\dagger Q_l R_l$. The expectation value of the Hamiltonian can therefore be obtained via:

$$\langle \psi | H_q | \psi \rangle = \sum_{l=0}^{m_c-1} \gamma_l \langle \psi | R_l^\dagger Q_l R_l | \psi \rangle. \quad (11)$$

This technique requires only m_c terms in the problem Hamiltonian to be estimated at the cost of implementing R_l within each quantum circuit. The following sections give both circuit constructions of R_l considered in this work. This follows the assembly outlined in [26].

A. Ordered sequence of rotations procedure

In this section, R_l is constructed such that it maps a completely anticommuting set H_{S_l} (equation 10) to a single Pauli operator via conjugation - formally: $R_l \left(\frac{H_{S_l}}{\gamma_l} \right) R_l^\dagger = P_n^{(l)}$. To begin a particular $P_j \in S_l$ is selected to be reduced to. This term is denoted by the index n and written as $P_n^{(l)}$, where l indexes the set. Once chosen, this operator is used to define the following set of Hermitian self-inverse operators [26]:

$$\{\mathcal{X}_{nk}^{(l)} = iP_n^{(l)} P_k^{(l)} \mid \forall P_k \in S_l \text{ where } k \neq n\}, \quad (12)$$

note the coefficients β_n and β_k are not present. As every P_j operator in S_l anticommutes with all other operators in the set by definition, it is clear from equation 12 that $\mathcal{X}_{nk}^{(l)}$ will commute with all $\{P_j \mid \forall P_j \in S_l \text{ where } j \neq n, k\}$ and anticommute with $P_n^{(l)}$ and $P_k^{(l)}$. This property is the crux of this conjugation approach. The adjoint rotation generated by $\mathcal{X}_{nk}^{(l)}$ can be written [26]:

$$R_{nk}^{(l)} = e^{\left(-i\frac{\theta_{nk}}{2}\mathcal{X}_{nk}^{(l)}\right)}, \quad (13)$$

whose action on H_{S_l} is [26]:

$$R_{nk}^{(l)} \left(\frac{H_{S_l}}{\gamma_l} \right) R_{nk}^{\dagger(l)} = (\beta_k \cos \theta_{nk} - \beta_n \sin \theta_{nk}) P_k^{(l)} + (\beta_k \sin \theta_{nk} + \beta_n \cos \theta_{nk}) P_n^{(l)} + \sum_{\substack{P_j \in S_l \\ \forall j \neq n, k}} \beta_j P_j. \quad (14)$$

The coefficient of $P_k^{(l)}$ can be made to go to 0, by setting $\beta_k \cos \theta_{nk} = \beta_n \sin \theta_{nk}$. This approach removes the term with index k and increases the coefficient of $P_n^{(l)}$ from $\beta_n \mapsto \sqrt{\beta_n^2 + \beta_k^2}$. This process is repeated over all indices excluding $k = n$ until only the $P_n^{(l)}$ term remains. This procedure can be concisely written using the following operator:

$$R_{S_l} = \prod_{\substack{k=0 \\ \forall k \neq n}}^{|H_{S_l}|-1} R_{nk}^{(l)}(\theta_{nk}), \quad (15)$$

which is simply a sequence of rotations. The angle θ_{nk} is defined iteratively at each step of the removal process, as the coefficient of $P_n^{(l)}$ increases at each step and thus must be taken into account. Importantly the correct solution for θ_{nk} must be chosen given the signs of β_n and β_k [26]. The overall action of this sequence of rotations is:

$$R_{S_l} \left(\frac{H_{S_l}}{\gamma_l} \right) R_{S_l}^{\dagger} = P_n^{(l)}. \quad (16)$$

Applying R_{S_l} on $\left(\frac{H_{S_l}}{\gamma_l} \right)$ by conjugation maps the unitary sum H_{S_l} to a single Pauli operator $P_n^{(l)}$ and unitary partitioning has been achieved. To summarise, in order to measure the expectation value of the Hamiltonian the following set of measurements are required:

$$\begin{aligned} H_q &= \sum_{i=0}^{m-1} c_i P_i = \sum_{l=0}^{m_c-1} H_{S_l} = \sum_{l=0}^{m_c-1} \gamma_l \left(\frac{H_{S_l}}{\gamma_l} \right) \\ &= \sum_{l=0}^{m_c-1} \gamma_l R_{S_l}^{\dagger} P_n^{(l)} R_{S_l}, \end{aligned} \quad (17)$$

where the number of terms in the qubit Hamiltonian requiring separate measurement is reduced from $m \mapsto m_c$. Note that $R_{S_l} \equiv R_l$, we use this notation to differentiate this assembly from the LCU construction.

B. Linear combination of unitaries method

1. LCU technique overview

Given a complex operator as a linear combination of d unitary operators:

$$A = \sum_{j=0}^{d-1} \alpha_j U_j, \quad \|A\| \leq \|\vec{\alpha}\|_1 = \sum_{j=1}^d |\alpha_j| \quad (18)$$

where U_j are unitary operators (that are assumed to be easy-to-implement) and α_j are real positive coefficients. Without loss of generality phase factors can be absorbed into the unitaries U_j to make all $\alpha_j \geq 0$. The linear combination of unitaries (LCU) method offers a way to probabilistically implement such an operator using the two unitary operators G and U_{LCU} [29, 45]:

$$U_{LCU} = \sum_{j=0}^{d-1} |j\rangle_a \langle j|_a \otimes U_j, \quad (19)$$

$$G = \sum_{j=0}^{d-1} \sqrt{\frac{\alpha_j}{\|\vec{\alpha}\|_1}} |j\rangle_a \langle 0|_a + \dots \quad (20)$$

where subscript a denotes the ancilla register. The most important property of the unitary operator G is that the coefficients α_j only define the first column of the matrix - resulting in $G|0\rangle_a \mapsto |G\rangle_a$. The rest of the columns must be orthogonal, but can have any values - hence there is a freedom of choice when defining G . A practical note on this is if one finds a quantum circuit that performs $|0\rangle_a \mapsto |G\rangle_a$, then its action on other basis states will automatically be accounted for and G is completely defined (provided the quantum circuit is composed as a product of unitaries). To summarise the LCU method, first G is used to initialize the ancilla register: $G|0\rangle_a \mapsto |G\rangle_a$. The controlled unitary U_{LCU} is then applied across the system and ancilla registers, resulting in [45]:

$$U_{LCU} |G\rangle_a |\psi\rangle_s \mapsto |G\rangle_a \frac{A}{\|\vec{\alpha}\|_1} |\psi\rangle_s + |G^\perp\rangle_a \sqrt{1 - \left\| \frac{A}{\|\vec{\alpha}\|_1} |\psi\rangle_s \right\|^2} |\psi\rangle_s. \quad (21)$$

If $|G\rangle_a$ is measured in the ancilla register, then the state will be projected onto $\frac{A}{\|\vec{\alpha}\|_1} |\psi\rangle_s$ and A was successfully applied to the system state $|\psi\rangle_s$. If any other state in the ancilla register is measured (orthogonal complement $\in \mathcal{H}_{G^\perp}$), then the quantum state is projected into the wrong part of the Hilbert space and $\frac{A}{\|\vec{\alpha}\|_1} |\psi\rangle_s$ is not performed.

The operator A is only implemented as a LCU with probability $(\frac{1}{\|\vec{\alpha}\|_1})^2$, hence the experiment will have to be repeated $\mathcal{O}(\frac{1}{p(\text{success})}) = \mathcal{O}((\|\vec{\alpha}\|_1)^2)$ times. Different techniques such as oblivious amplitude amplification [41] and amplitude amplification [42, 43] can be used to boost the success probability however, extra coherent resources are required.

An alternate way to describe the LCU method is to note that the matrix A is in general not unitary. To build a unitary form, the normalised matrix A can be embedded into a larger Hilbert space by putting it into the upper-left block of a unitary matrix:

$$U_{LCU} = \begin{bmatrix} \frac{A}{\|\vec{\alpha}\|_1} & \cdot \\ \cdot & \cdot \end{bmatrix}, \quad (22)$$

where each $[\cdot]$ represents a matrix of arbitrary elements. The operator U_{LCU} is a probabilistic implementation of A and is commonly known as a ‘block encoding’ of A . Overall the LCU method encodes the desired matrix as [45]:

$$\langle G|_a U_{LCU} |G\rangle_a = \frac{A}{\|\vec{\alpha}\|_1}. \quad (23)$$

The LCU technique can be used to implement non-unitary operations [29, 46], such as matrix inversion. This is achieved by constructing the required operator as a linear combination of unitaries. For example, the n -fold tensor product of Pauli operators including the n -fold identity operation form a basis for the space of all $(2^n \times 2^n)$ matrices and thus any $(2^n \times 2^n)$ operator can be built by different linear combinations of these unitary operators.

A toy example of the LCU method is given in the next section to illustrate the practical implementation of this technique. This can be skipped without loss of continuity.

2. Toy LCU example

Consider the Hamiltonian $H = \alpha_0 U_0 + \alpha_1 U_1$, where $\alpha_{0,1} \geq 0$ and $\|\vec{\alpha}\|_1 = |\alpha_0| + |\alpha_1|$. To implement this operator as a linear combination of unitaries G (equation 20) and U_{LCU} (equation 19) must be defined. The construction of these operators is given by the definition of H . In this case, they will be:

$$U_{LCU} = (|0\rangle_a \langle 0|_a \otimes U_0) + (|1\rangle_a \langle 1|_a \otimes U_1), \quad (24)$$

$$\begin{aligned} G &= \sqrt{\frac{\alpha_0}{\|\vec{\alpha}\|_1}} |0\rangle_a \langle 0|_a + \sqrt{\frac{\alpha_1}{\|\vec{\alpha}\|_1}} |1\rangle_a \langle 0|_a \\ &\quad x |0\rangle_a \langle 1|_a + y |1\rangle_a \langle 1|_a, \\ &= \begin{bmatrix} \sqrt{\frac{\alpha_0}{\|\vec{\alpha}\|_1}} & x \\ \sqrt{\frac{\alpha_1}{\|\vec{\alpha}\|_1}} & y \end{bmatrix}. \end{aligned} \quad (25)$$

The values of x and y can be anything that ensures the columns of G are orthogonal. The following can be used:

$$\begin{aligned} G &= \sqrt{\frac{\alpha_0}{\|\vec{\alpha}\|_1}} |0\rangle_a \langle 0|_a + \sqrt{\frac{\alpha_1}{\|\vec{\alpha}\|_1}} |1\rangle_a \langle 0|_a \\ &\quad - \sqrt{\frac{\alpha_1}{\|\vec{\alpha}\|_1}} |0\rangle_a \langle 1|_a + \sqrt{\frac{\alpha_0}{\|\vec{\alpha}\|_1}} |1\rangle_a \langle 1|_a, \\ &= \begin{bmatrix} \sqrt{\frac{\alpha_0}{\|\vec{\alpha}\|_1}} & -\sqrt{\frac{\alpha_1}{\|\vec{\alpha}\|_1}} \\ \sqrt{\frac{\alpha_1}{\|\vec{\alpha}\|_1}} & \sqrt{\frac{\alpha_0}{\|\vec{\alpha}\|_1}} \end{bmatrix}, \end{aligned} \quad (26)$$

as discussed in [46]. The quantum circuit given in Fig.4 shows the probabilistic implementation of H using the LCU method. Stepping through this circuit we find:

$$\begin{aligned} \text{(i)} \quad & |0\rangle_a |\psi\rangle_s \xrightarrow{G \otimes \mathcal{I}_s} \frac{1}{\sqrt{\|\vec{\alpha}\|_1}} (\sqrt{\alpha_0} |0\rangle_a + \sqrt{\alpha_1} |1\rangle_a) |\psi\rangle_s \\ \text{(ii)} \quad & |0\rangle_a \langle 0|_a \otimes U_0 \xrightarrow{\frac{1}{\sqrt{\|\vec{\alpha}\|_1}}} (\sqrt{\alpha_0} |0\rangle_a U_0 |\psi\rangle_s + \sqrt{\alpha_1} |1\rangle_a |\psi\rangle_s) \\ & |1\rangle_a \langle 1|_a \otimes U_1 \xrightarrow{\frac{1}{\sqrt{\|\vec{\alpha}\|_1}}} (\sqrt{\alpha_0} |0\rangle_a U_0 |\psi\rangle_s + \sqrt{\alpha_1} |1\rangle_a U_1 |\psi\rangle_s) \\ \text{(iii)} \quad & G^\dagger \otimes \mathcal{I}_s \xrightarrow{\frac{1}{\|\vec{\alpha}\|_1}} \left(|0\rangle_a (\alpha_0 U_0 + \alpha_1 U_1) |\psi\rangle_s + \sqrt{\alpha_0 \alpha_1} |1\rangle_a (U_1 - U_0) |\psi\rangle_s \right). \end{aligned}$$

Measuring $|0\rangle_a$ on the ancilla line will project the state onto $(\alpha_0 U_0 + \alpha_1 U_1) |\psi\rangle_s = H |\psi\rangle_s$ and heralds a successful implementation of the linear combination of unitaries method. If $|1\rangle_a$ is measured then the state is projected into the wrong subspace and H is not performed.

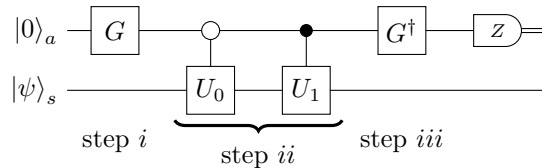


FIG. 4: Quantum circuit to implement $H = \alpha_0 U_0 + \alpha_1 U_1$ as a linear combination of unitaries.

3. LCU approach to unitary partitioning

Analogous to the sequence of rotations method (Section I A), R_l will be applied by conjugation to an anticommuting set H_{S_l} to give a single Pauli operator. However, unlike the previous method, where R_l was achieved by a sequence of rotations (equation 15) here it is built via a linear combination of unitaries (LCU). An overview of the LCU method is given in Section I B 1.

To construct R_l via LCU, we first need to manipulate each of the m_c anticommuting sets (H_{S_l}) that the qubit Hamiltonian was partitioned into (equation 9). As before, a particular Pauli operator $P_j \in S_l$ in each set is selected to be reduced to. Again this will be denoted by the index n and written as $P_n^{(l)}$, where l indexes the set. At this point constructions of R_l diverge. To begin we define the operator $H_{S_l \setminus \{P_n^{(l)}\}}$:

$$H_{S_l \setminus \{P_n^{(l)}\}} = \sum_{\substack{\forall k \neq n \\ |H_{S_l}|-1}} \delta_k P_k, \quad (27a)$$

$$\text{where } \sum_{\substack{j=0 \\ \forall j \neq n}}^{|H_{S_l}|-1} \delta_k^2 = 1. \quad (27b)$$

Taking each normalised set H_{S_l} (equation 10) and re-writing them with the term we are reducing to ($\beta_n^{(l)} P_n^{(l)}$) outside the sum:

$$\frac{H_{S_l}}{\gamma_l} = \beta_n^{(l)} P_n^{(l)} + \sum_{\substack{j=0 \\ \forall j \neq n}}^{|H_{S_l}|-2} \beta_j^{(l)} P_j^{(l)}, \quad (28)$$

by re-normalising the remaining sum in equation 28:

$$\frac{H_{S_l}}{\gamma_l} = \beta_n^{(l)} P_n^{(l)} + \Omega_l \sum_{\substack{j=0 \\ \forall j \neq n}}^{|H_{S_l}|-2} \delta_j^{(l)} P_j^{(l)}, \quad (29a)$$

$$\text{where } \sum_{\substack{j=0 \\ \forall j \neq n}}^{|H_{S_l}|-2} \delta_j^{2(l)} = 1, \quad (29b)$$

$$\text{and } \beta_j^{(l)} = \Omega_l \delta_j^{(l)}. \quad (29c)$$

We can substitute equation 27 into equation 29:

$$\frac{H_{S_l}}{\gamma_l} = \beta_n^{(l)} P_n^{(l)} + \Omega_l H_{S_l \setminus \{P_n^{(l)}\}}, \quad (30)$$

where $\beta_n^{2(l)} + \Omega_l^2 = 1$. In this form we can use the trigonometric identity $\cos^2(\theta) + \sin^2(\theta) = 1$ to define the following operator:

$$H_n^{(l)} = \cos(\phi_n^{(l)}) P_n^{(l)} + \sin(\phi_n^{(l)}) H_{S_l \setminus \{P_n^{(l)}\}}. \quad (31)$$

Comparing equations 30 and 31 it is clear that $\cos(\phi_n^{(l)}) = \beta_n^{(l)}$ or $\sin(\phi_n^{(l)}) = \Omega_l$. Next using the definition of $H_n^{(l)}$ in equation 31 it was shown in [26] that one can consider rotations of H_n around an axis that is Hilbert-Schmidt orthogonal to both $H_{S_l \setminus \{P_n^{(l)}\}}$ (equation 27) and $P_n^{(l)}$:

$$\mathcal{X}^{(l)} = \frac{i}{2} [H_{S_l \setminus \{P_n^{(l)}\}}, P_n^{(l)}] = i \sum_{\substack{k=0 \\ \forall k \neq n}}^{|H_{S_l}|-2} \delta_k^{(l)} P_k^{(l)} P_n^{(l)}. \quad (32)$$

$\mathcal{X}^{(l)}$ anticommutes with $H_n^{(l)}$, is self-inverse and has the following action [26]:

$$\mathcal{X}^{(l)} H_n^{(l)} = i(-\sin \phi_n^{(l)} P_n^{(l)} + \cos \phi_n^{(l)} H_{S_l \setminus \{P_n^{(l)}\}}). \quad (33)$$

This defines the rotation:

$$R_l = e^{(-i \frac{\alpha^{(l)}}{2} \mathcal{X}^{(l)})} = \cos\left(\frac{\alpha^{(l)}}{2}\right) \mathcal{I} - i \sin\left(\frac{\alpha^{(l)}}{2}\right) \mathcal{X}^{(l)} \quad (34a)$$

$$= \cos\left(\frac{\alpha^{(l)}}{2}\right) \mathcal{I} - i \sin\left(\frac{\alpha^{(l)}}{2}\right) \left(i \sum_{\substack{k=0 \\ \forall k \neq n}}^{|H_{S_l}|-2} \delta_k^{(l)} P_k^{(l)} P_n^{(l)} \right) \quad (34b)$$

$$= \cos\left(\frac{\alpha^{(l)}}{2}\right) \mathcal{I} + \sin\left(\frac{\alpha^{(l)}}{2}\right) \sum_{\substack{k=0 \\ \forall k \neq n}}^{|H_{S_l}|-2} \delta_k^{(l)} P_{kn}^{(l)}, \quad (34c)$$

where $P_k^{(l)} P_n^{(l)} = P_{kn}^{(l)}$. Importantly $P_{kn}^{(l)}$ will be another tensor product of Pauli operators, as products of n -fold Pauli operators will yield another operator in the Pauli group. The adjoint action of this rotation on $H_n^{(l)}$ is:

$$R_l H_n^{(l)} R_l^\dagger = \sin(\phi_n^{(l)} - \alpha^{(l)}) H_{S_l \setminus \{P_n^{(l)}\}} + \cos(\phi_n^{(l)} - \alpha^{(l)}) P_n^{(l)}. \quad (35)$$

By setting $\alpha^{(l)} = \phi_n^{(l)}$, the coefficient of $H_{S_l \setminus \{P_n^{(l)}\}}$ will go to zero and we achieve the intended result of $R_l H_n^{(l)} R_l^\dagger = P_n^{(l)}$. To build R_l by the LCU method, we use its definition in equation 34c. In practice, it is easier to re-write equation 34 using the fact that all P_{kn} and \mathcal{I} are in the Pauli group. The terms can thus be combined into a single sum:

$$R_l = \alpha \mathcal{I} + \sum_{\substack{k=0 \\ \forall k \neq n}}^{|H_{S_l}|-2} \alpha_k P_{kn}^{(l)} \quad (36a)$$

$$= \sum_{\substack{q=0 \\ \forall q \neq n}}^{|H_{S_l}|-1} \alpha_q P_q^{(l)}. \quad (36b)$$

When written in this form, it is easy to define the operators G (equation 20) and U_{LCU} (equation 19):

$$G = \sum_{q=0}^{|H_{S_l}|-1} \sqrt{\frac{\alpha_q}{\|\vec{\alpha}_q\|_1}} |q\rangle_a \langle 0|_a + \dots \quad (37)$$

$$U_{LCU} = \sum_{q=0}^{|H_{S_l}|-1} |q\rangle_a \langle q|_a \otimes P_q, \quad (38)$$

that are required to perform R_l as a LCU. Overall the operator is encoded as:

$$\langle 0|_a G^\dagger U_{LCU} G |0\rangle_a = \langle G|_a U_{LCU} |G\rangle_a = \frac{R_l}{\|\vec{\alpha}_q\|_1}. \quad (39)$$

Without using amplitude amplification, the probability of success is given by the square of the l_1 -norm of R_l - denoted as $(\|\vec{\alpha}_q\|_1)^2$. Note that the l_1 -norm is defined as $\|\vec{\alpha}_q\|_1 = \sum_{q=0}^{|H_{S_l}|-1} |\alpha_q|$.

II. CIRCUIT DEPTH ANALYSIS

In order to investigate the circuit depth of each technique, we consider circuits made up of arbitrary single qubit and CNOT gates. As will be seen in the following sections, in general the LCU method has a much greater gate count. However, different scaling measures often consider a universal gate set - such as Clifford and T gates - when analysing fault-tolerant protocols. The LCU method only requires arbitrary rotations in the operator G , whereas the sequence of rotations method requires many more. The relative depth of LCU vs sequence of rotations circuits would be interesting to explore in this setting.

A. Sequence of rotations implementation

To construct the quantum circuit for R_{S_l} (equation 15) we need to consider the cost to perform each $R_{n_k}^{(l)}$ rotation (equation 13). Whitfield *et al.* in [47] show how to build the required quantum circuits for these types of operators and an example is illustrated in Fig.5. Every $R_{n_k}^{(l)}$ circuit will therefore require $\mathcal{O}(2(N_s - 1))$ CNOT gates, 1 $R_z(\theta)$ gate and $\mathcal{O}(2N_s)$ change of basis gates $\{H, R_x(\theta)\}$. Here N_s is the number of system qubits. A single $R_{n_k}^{(l)}$ is needed for each term in the set S_l , apart from for $P_n^{(l)}$. The total number of rotations that make up the full sequence of rotation operator R_{S_l} is therefore $|H_{S_l}| - 1$. $|H_{S_l}|$ is the size of the anticommuting set. The overall gate count scales as $\mathcal{O}((2N_s + 1)(|H_{S_l}| - 1))$ single qubit and gates and $\mathcal{O}(2(N_s - 1)(|H_{S_l}| - 1))$ CNOT gates.

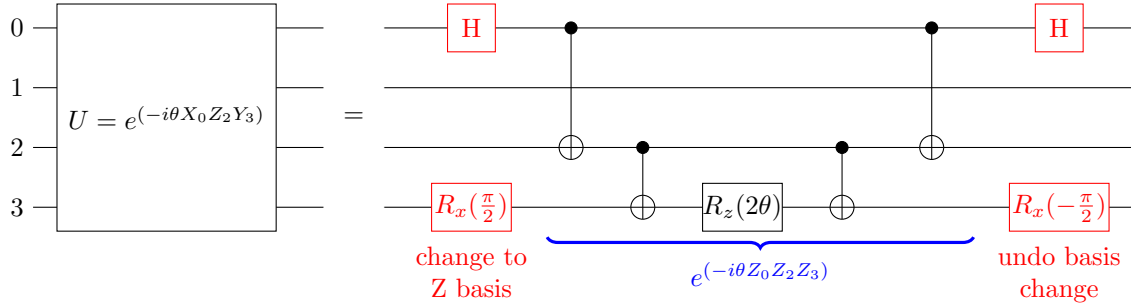


FIG. 5: Quantum circuit to perform a unitary operator given as an exponentiated n -fold tensor product of Pauli operators [47].

B. LCU implementation

For the linear combination of unitaries approach to unitary partitioning, we need to consider the gates required to realise G (equation 37) and U (equation 38). We will not explicitly consider the construction of G , as it heavily depends on the ancilla state required and many different approaches are possible. In the worst case, without introducing any additional qubits, $\mathcal{O}(N \log_2(N)^2)$ standard 1 and 2-bit gate operations are required [48]. On the other hand, the quantum circuit to construct U_{LCU} is well defined. U_{LCU} is made up by a control version of each P_q given in equation 36. Ancilla qubits are therefore necessary for the control lines and the number required is given by the number of operators U_{LCU} is constructed from. In this case, the number of ancilla qubits N_a equals $\lceil \log_2(|H_{S_i}| - 1) \rceil$. Overall, $(|H_{S_i}| - 1) N_a$ -bit controlled P_q gates are required. To efficiently construct each control P_q gate, $N_a - 1$ work qubits are employed. The control states of the ancilla qubits are stored on these work qubits using Toffoli gates [49]. An example is shown in Fig.6. For every control P_i a cascade of $\mathcal{O}(2(N_c - 1))$ Toffoli gates are required. Importantly if we arrange the sequence of control gates optimally, we can reuse some of the work qubits when the control states overlap. Fig.7 and Fig.8 show different possible circuit reductions for a Grey and binary sequence of controls.

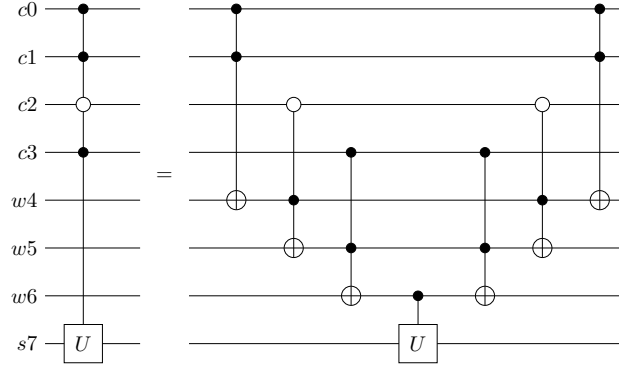


FIG. 6: Example quantum circuit required to perform 4-bit controlled U gate [49]. Note that c, w, s denote control, work and system qubits respectively.

To understand the circuit depth we consider all possible 2^{N_c} control states, where N_c is the number of control qubits. By ordering the control bitstrings in a Grey code, each sequence will only differ by one bit [52]. The largest circuit simplification occurs when only the control bit on the lowest control line differs. In this scenario, we get the reduction given in Fig.7a for all the Toffoli gates in-between the two control unitaries apart from the final two gates, which must differ by one bit due to the Grey encoding. The identity given in Fig.7b is applied to reduce this case to a CNOT gate. This occurs every other control gate in a Grey code - or 2^{N_c-1} times. For control instances where the bitstrings differ by bits above the lowest control line a partial reduction occurs. The amount is dependent on how many bitstrings are in common above the lowest common control line. In general, for x bits in common above there will be a reduction to identify (Fig.7a) 2^{N_c-x} times followed by a single application of Fig.7b, where $2 \leq x < (N_c)$. Again, as the bitstrings follow a Grey encoding the identity in Fig.8a can always be applied once to each case. Finally, if there are over 2^{N_c-1} control states, there must be a single case when the top control bit differs ($x = N_c$). In this

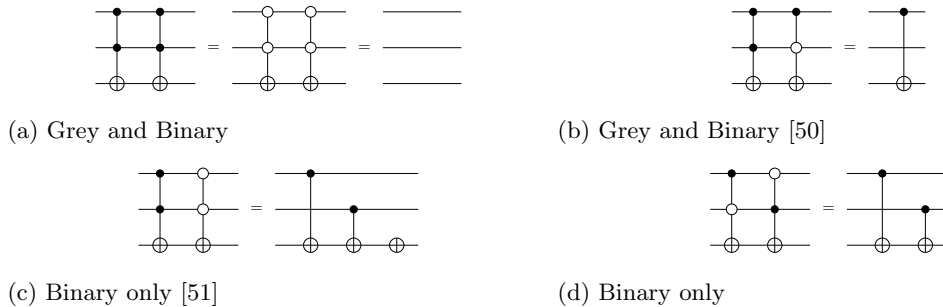


FIG. 7: Toffoli-Toffoli circuit templates

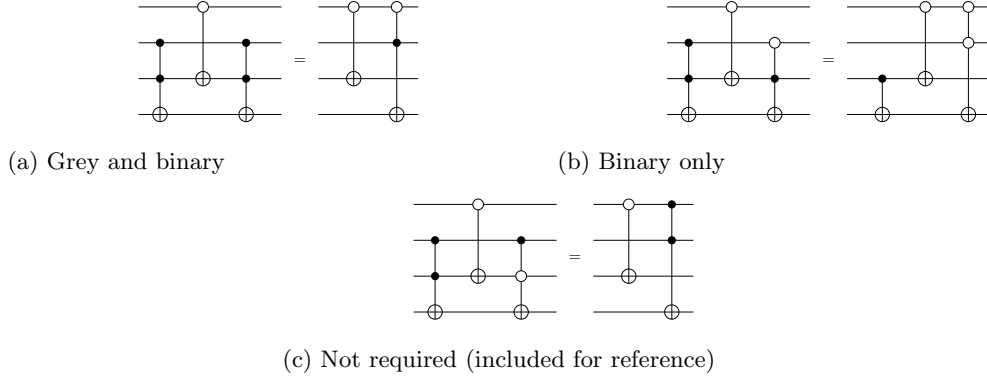


FIG. 8: Toffoli-CNOT-Toffoli circuit templates

scenario no reduction to identity (Fig.7a) is possible and only Fig.7b can be applied followed by Fig.8a. These rules and circuit templates can be used to find different reductions. The choice of control states determines the overall gate count.

When all the control states of a Grey code are required and no freedom of control state choice is possible, the circuit scales as $\mathcal{O}(2^{N_c}(2N_c - 2))$ Toffoli gates with no simplifications. Using a Grey code, the circuits can be simplified - the Toffoli count required scales as $\mathcal{O}(3(2^{N_c-1}) - 5)$, with $\mathcal{O}(2^{N_c} - 1)$ additional CNOT gates. An example of this approach can be seen across the control and work qubit registers of Fig.11, where the number of control bits is 3 and all 8 control strings are present.

Each Toffoli gate can be decomposed into 9 single qubit gates and 6 CNOT gates [53], therefore the reduced gate count requires $\mathcal{O}(27(2^{N_c-1}) - 45)$ single qubit gates and $\mathcal{O}(5(2^{N_c+1}) - 31)$ CNOT gates. These counts do not include any gate that acts on the system register, as different approaches are possible. In the next two Sections we analyse two different possibilities - a cascade and direct approach.

1. LCU cascade

In the cascade approach, each Pauli operator in every control- P_i gate of U_{LCU} (equation 38) must undergo a change of basis, requiring $\mathcal{O}(2N_s)$ gates. An example is shown in Fig.9.

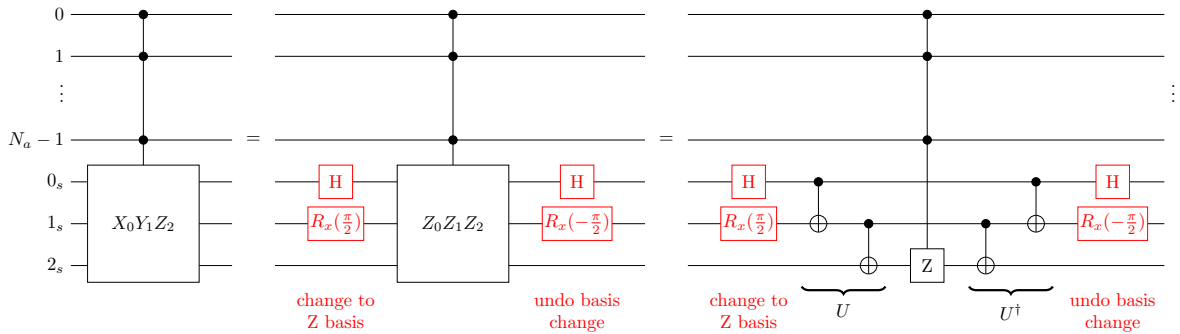


FIG. 9: Example quantum circuit to perform a multi-control P_i gate via a cascade approach. Here: $Z_0 \otimes Z_1 \otimes Z_2 = U(\mathcal{I}_0 \otimes \mathcal{I}_1 \otimes Z_2)U^\dagger$.

A cascade of $\mathcal{O}(2(N_s - 1))$ CNOT gates can be used to convert the multi-controlled n -fold Z gate into an n -bit Z gate. Two Hadamard gates can convert this into an n -bit Toffoli. Continuing the example in Fig.9, we get Fig.10.

The additional gate count on the system register will scale as $\mathcal{O}(2^{N_c}(2N_s+2))$ single qubit gates and $\mathcal{O}(2^{N_c}(2N_s-1))$ CNOT gates. The full gate count, including the ancilla register, scales as $\mathcal{O}(2^{N_c-1}(4N_s + 31) - 45)$ single qubit gates and $\mathcal{O}(2^{N_c}(2N_s + 9) - 31)$ CNOT gates. Importantly $N_c = \lceil \log_2(|H_{S_I}| - 1) \rceil$ and $N_w = N_c - 1$. An example case for $N_c = 3$ is given in Fig.11.

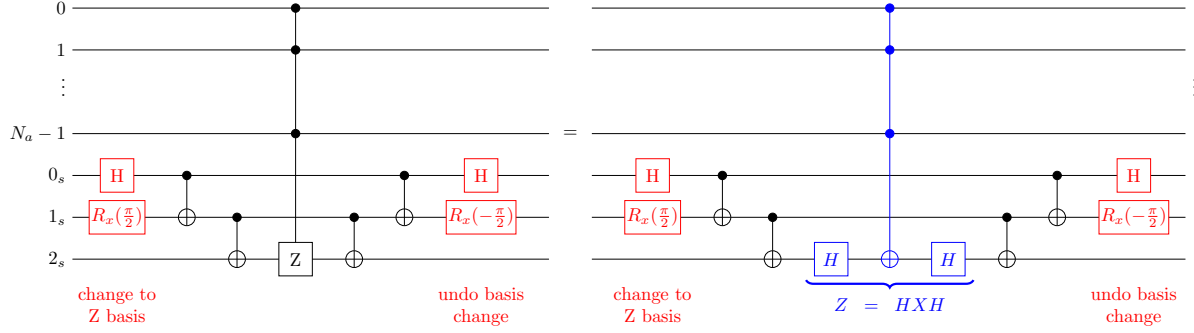


FIG. 10: Continued quantum circuit example from Fig.9. Illustrates conversion of n -bit control Z gate to an n -bit Toffoli gate.

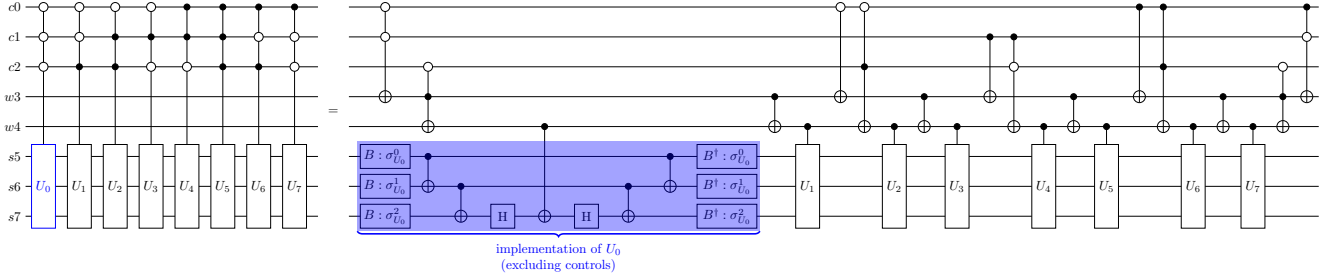


FIG. 11: Example quantum circuit to perform U_{LCU} via the cascade approach. The single qubit B gates are required to perform a change of basis dependent on the Pauli operators in each U_i operator. Only the system register deconstruction for U_0 has been shown here (blue). Note that c, w, s denote control, work and system qubits respectively.

2. LCU direct

Compared to the cascade approach (Section II B 1), the direct approach implements each control n -fold Pauli operator of U_{LCU} (equation 38) on the system register directly. $\mathcal{O}(2N_s)$ change of basis gates and $\mathcal{O}(N_s)$ CNOT gates are required per control gate. The number of single and CNOT gates scales as $\mathcal{O}(2N_s(2^{N_c}))$ and $\mathcal{O}(N_s(2^{N_c}))$ respectively. The overall gate count over the system and ancilla registers scales as $\mathcal{O}(2^{N_c-1}(2N_s + 27) - 45)$ single qubit gates and $\mathcal{O}(2^{N_c}(N_s + 10) - 31)$ CNOT gates. A full example for $N_c = 3$ is presented in Fig.12.

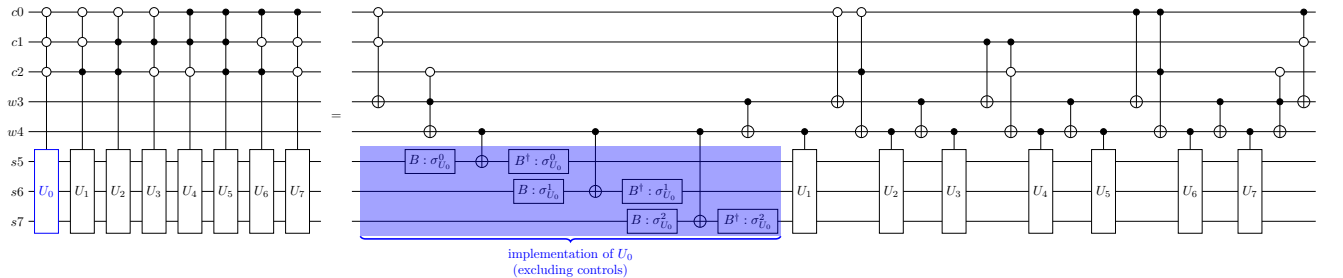


FIG. 12: Example quantum circuit to perform U_{LCU} via the direct approach. The single qubit B gates are required to perform a change of basis dependent on the Pauli operators in each U_i operator. Only the system register deconstruction for U_0 has been shown here (blue). Note that c, w, s denote control, work and system qubits respectively.

3. LCU constant factor ($|H_{S_l}| \leq 5$)

The scaling is different when $N_c \leq 2$ and no work qubits are required. For $N_c = 1$ all gates in U_{LCU} are controlled by one ancilla qubit. The G gate (equation 37) is defined by a single R_y rotation and each unitary in U_{LCU} (equation 38) is implemented by $\mathcal{O}(4(N_s))$ change of basis gates and $\mathcal{O}(2N_s)$ CNOT gates.

For $N_c = 2$, the direct and cascade approach can be used to construct U_{LCU} . The direct approach requires $\mathcal{O}(4N_s)$ Toffoli and $\mathcal{O}(8N_s)$ change of basis gates. The cascade approach requires $\mathcal{O}(8N_s)$ changes of basis, $\mathcal{O}(8N_s)$ CNOT and $\mathcal{O}(4)$ Toffoli gates.

The greatest measurement reduction is obtained if the minimum clique cover is found. This cover has the fewest H_{S_l} sets possible. However, non-optimal clique covers still give a measurement reduction. For problems where the minimum clique cover has anticommuting cliques $|H_{S_l}| > 5$, it can be beneficial to split these up into smaller sets such that $|H_{S_l}| \leq 5 \forall \{l\}_{l=0,1,\dots,m_c-1}$. As discussed above, no work qubits will now be required to implement R_l and the circuits required to implement unitary partitioning are experimentally realistic for current and near term devices. This offers a constant factor improvement on the number of measurements required.

4. Further LCU simplifications

An additional circuit simplification, is possible cancellations in the gates making up U_{LCU} . We did not explicitly consider this in our work here, but note its clear application. The ordering of the control unitaries in U_{LCU} is arbitrary and common qubit-wise Pauli strings can be cancelled. The optimal reduction is obtained if Pauli operators on common qubits are maximised - this is known as a lexicographical ordering. An example is given in Fig.13.

We did not employ this process for our H_2 simulation, as it offered no improvement. The LiH problem would have benefited from this reduction however, as we only simulated this problem on a QPU emulator multi-control gates could be performed directly. We therefore didn't decompose these operations into their single and two qubit gates and simulated the control P_i gates directly.

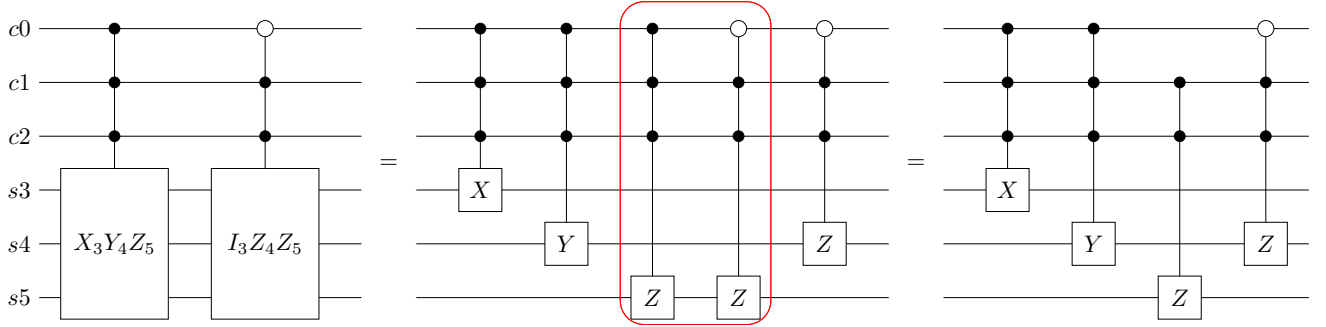
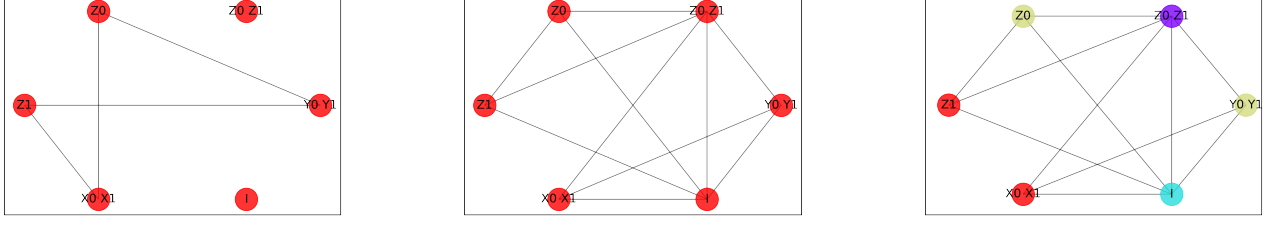


FIG. 13: Example lexicographical circuit simplification.

III. NUMERICAL STUDY

The ability of the unitary partitioning measurement reduction strategy is dependent on the problem Hamiltonian. To understand the performance of these methods we investigate Hamiltonians of interest in quantum chemistry. We consider Hamiltonians for H_2 and LiH molecules, each obtained using Openfermion-PySCF [30, 31]. These were converted into the qubit Hamiltonian using the Bravyi-Kitaev transformation in OpenFermion [30]. The following Sections give numerical details.



(a) Graph of qubit Hamiltonian of H_2 (equation 41) with anticommuting terms joined by edges

(b) Complementary graph of (a)

(c) Clique cover of (a) found by graph colouring of complementary graph (b)

FIG. 14: Illustration of graph approach to finding anticommuting sets of P_i operators.

A. Molecular Hydrogen

In the minimal STO-3G basis the qubit Hamiltonian for H_2 in the BK representation is:

$$H_q^{(H_2)} = c_0 \mathcal{I} + c_1 X_0 Z_1 X_2 + c_2 X_0 Z_1 X_2 Z_3 + c_3 Y_0 Z_1 Y_2 + c_4 Y_0 Z_1 Y_2 Z_3 + c_5 Z_0 + c_6 Z_0 Z_1 + c_7 Z_0 Z_1 Z_2 + c_8 Z_0 Z_1 Z_2 Z_3 + c_9 Z_0 Z_2 + c_{10} Z_0 Z_2 Z_3 + c_{11} Z_1 + c_{12} Z_1 Z_2 Z_3 + c_{13} Z_1 Z_3 + c_{14} Z_2. \quad (40)$$

This Hamiltonian only acts off diagonally on qubits 0 and 2 [54], therefore it can be reduced to:

$$H_q^{(H_2)} = (c_0 + c_{11} + c_{13}) \mathcal{I} + (c_1 + c_2) X_0 X_2 + (c_3 + c_4) Y_0 Y_2 + (c_5 + c_6) Z_0 + (c_7 + c_8 + c_{10}) Z_0 Z_2 + (c_9 + c_{12} + c_{14}) Z_2. \quad (41)$$

Overall 2 qubits are required, and the terms with indices 2 are re-labelled with indices of 1. The input state was found by diagonalising the problem Hamiltonian (Equation 41) - $|\psi_{H_2}^{ground}\rangle = -0.1125|01\rangle + 0.9936|10\rangle$. For our calculation, the bond length was set to $R(\text{H-H})=0.74 \text{ \AA}$. Note that we index the state from left to right.

To perform unitary partitioning, the qubit Hamiltonian for H_2 needs to be split into anticommuting sets H_{S_l} (equation 10). To do this the NetworkX package was used [32]. First, a graph of the qubit Hamiltonian was built, where each node is a term in the Hamiltonian. Next edges are put between nodes on the graph that anticommute. Finally, a graph colouring of the complement graph was performed. This searches for the minimum number of colours required to colour the graph, where no neighbours of a node can have the same color as the node itself. The “largest first” colouring strategy in NetworkX was used. Each unique colour represents an anticommuting clique. Fig.14 shows the method applied to H_2 and Table I gives the resulting anticommuting sets H_{S_l} obtained. Note the set index l represents a unique colour obtained in the graph colouring. This approach is the minimum clique cover problem mapped to a graph colouring problem.

The following subsections give the quantum circuits used to estimate the ground state of H_2 by standard VQE, and VQE with unitary partitioning applied.

l index	H_{S_l}
0	$(0.5731061703432151 + 0j) Z_0 Z_1$
1	$(0.2460355896585992 + 0j) I_0 I_1$
2	$\{(-0.4468630738162712 + 0j) I_0 Z_1, (0.09060523100759853 + 0j) X_0 X_1\}$
3	$\{(0.3428256528955378 + 0j) Z_0 I_1, (0.09060523100759853 + 0j) Y_0 Y_1\}$

TABLE I: Qubit Hamiltonian for H_2 (equation 41) at a bond length of 0.74 \AA partitioned into anticommuting sets (Equation 9)

1. Sequence of rotations quantum circuits

l index	γ_l	P_n	\mathcal{X}_{nk}	θ_{nk}
2	0.455956044621043	$(1)Z_1$	$(-1)X_0Y_1$	2.941546221798205
3	0.35459658228639496	$(1)Z_0$	$(1)X_0Y_1$	0.25838176362668025

TABLE II: Given the partitioning in Table I, this table gives the operators and angles required to build R_{S_l} (equation 15) as a sequence of rotations.

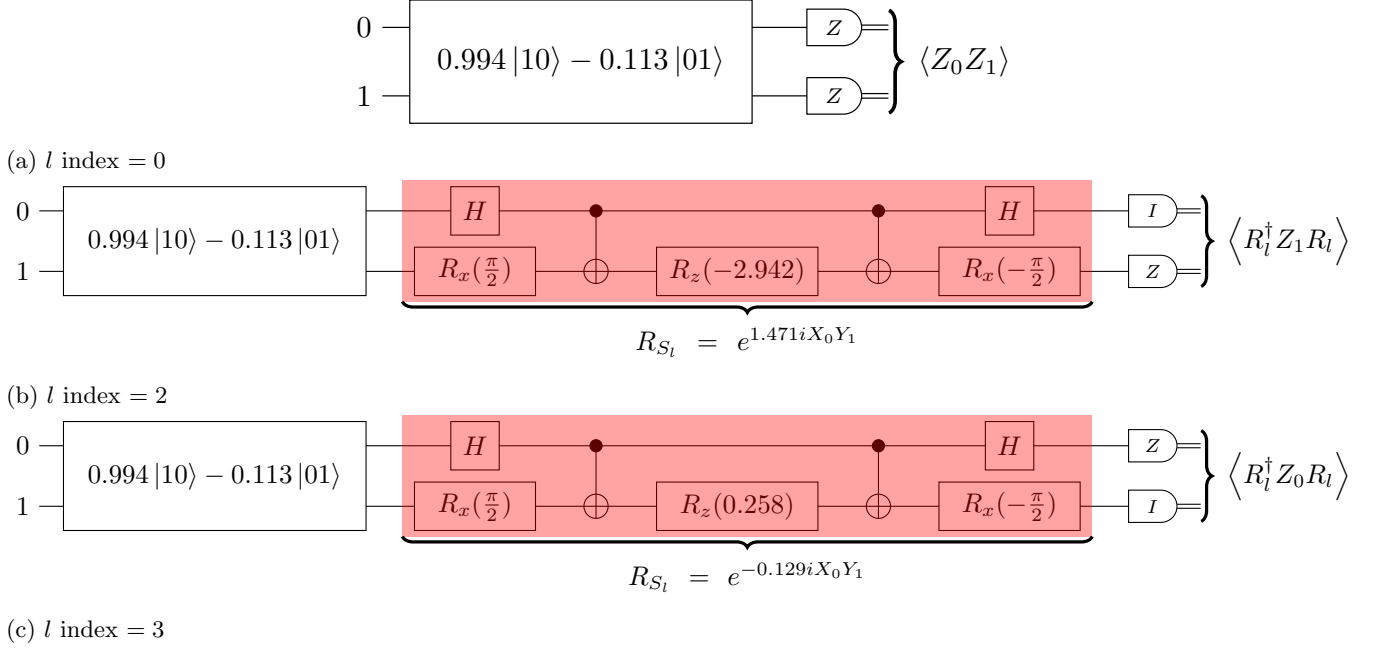


FIG. 15: Quantum circuits required to find the ground state of H_2 using VQE with unitary partitioning applied as a sequence of rotations. Tables I and II define all operators required.

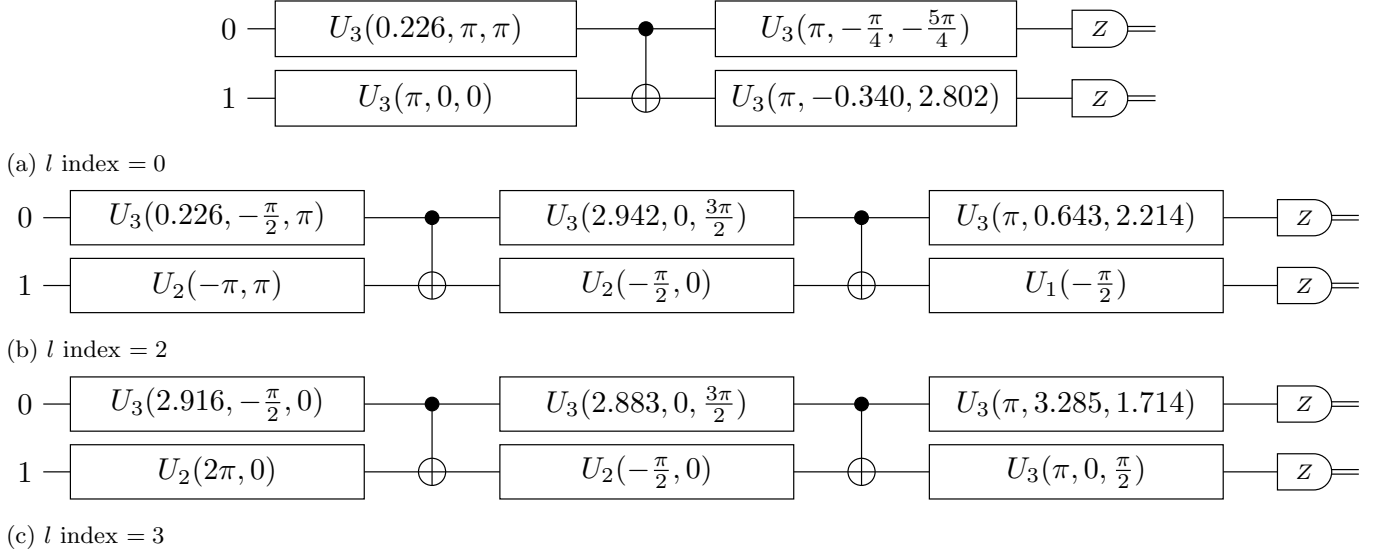


FIG. 16: Quantum circuits required to find the ground state of H_2 using VQE with unitary partitioning applied as a sequence of rotations. Tables I and II define all operators required. These circuits are the compiled versions of those in Fig. 15 for use on IBM's QPU.

2. LCU quantum circuits

l index	γ_l	P_n	$R_l = \sum_q \alpha_q^{(l)} P_q^{(l)}$	$U_{LCU}^{(l)} = \sum_q q\rangle_a \langle q _a \otimes P_q^{(l)}$	$ G\rangle_a = \sum_q \sqrt{\frac{ \alpha_q }{\ \alpha\ _1}} q\rangle_a$
2	0.455956044621043	$(1)Z_1$	$(0.09985651653293749)I +$ $(0.9950018472876858i)X_0Y_1$	$ 0\rangle_a \langle 0 _a \otimes I +$ $ 1\rangle_a \langle 1 _a \otimes 1i X_0Y_1$	$(0.3020015943219478) 0\rangle_a +$ $(0.9533074199999713) 1\rangle_a$
3	0.35459658228639496	$(1)Z_0$	$(0.9916664584717437)I +$ $(-0.12883180951189593i)X_0Y_1$	$ 0\rangle_a \langle 0 _a \otimes I +$ $ 1\rangle_a \langle 1 _a \otimes -1i X_0Y_1$	$(0.9407564775082788) 0\rangle_a +$ $(0.3390829544908076) 1\rangle_a$

TABLE III: Given the partitioning in Table I, this table gives the operators and ancilla states required to build R_l (equation 36) as a linear combination of unitaries.

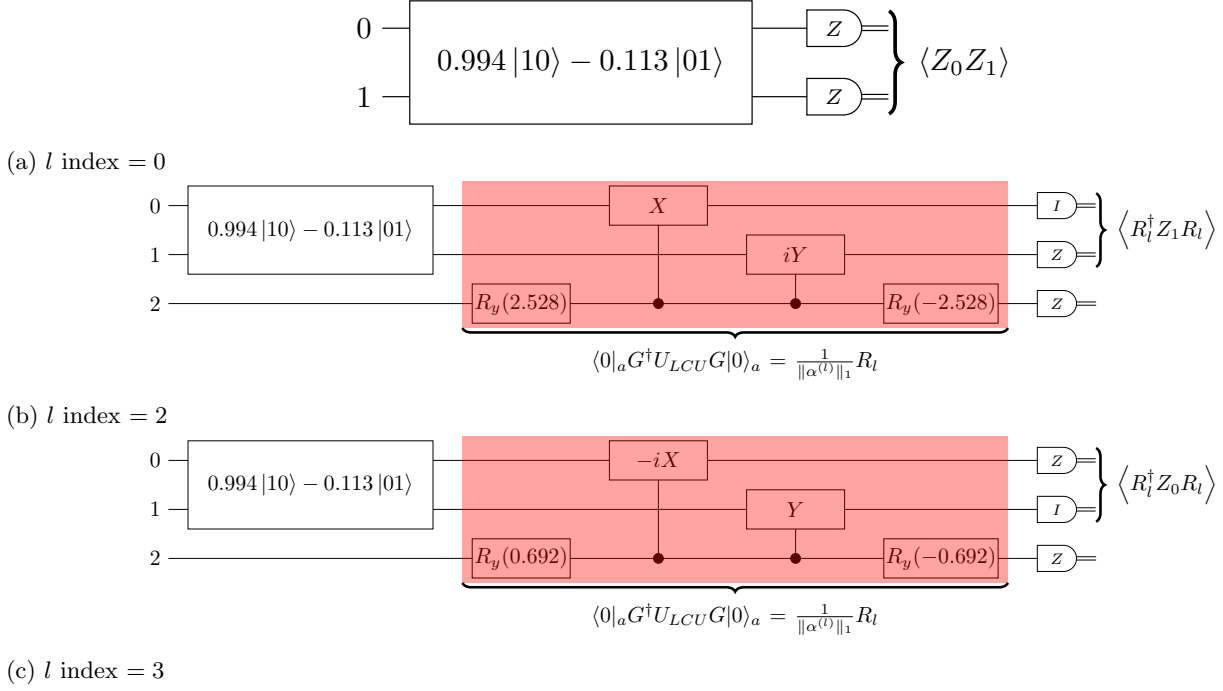


FIG. 17: Quantum circuits required to find the ground state of H_2 using VQE with unitary partitioning applied as a LCU. Tables I and III define all operators and states $|G\rangle$ required.

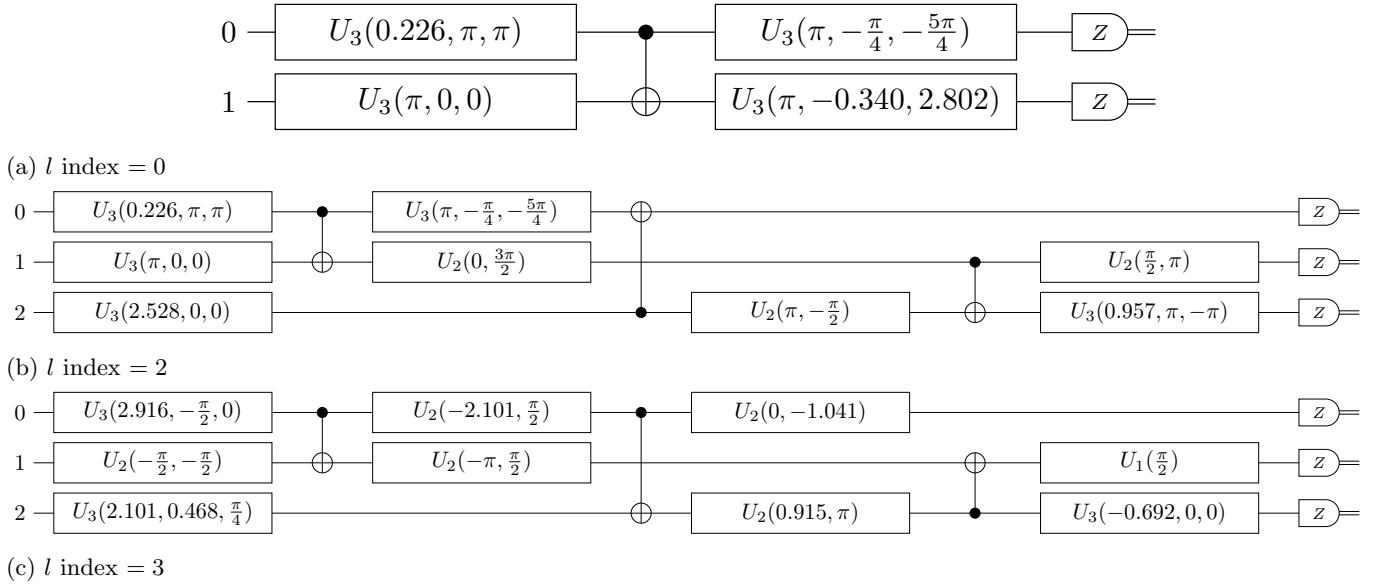


FIG. 18: Quantum circuits required to find the ground state of H_2 using VQE with unitary partitioning applied as a LCU. Tables I and III define all operators and states $|G\rangle$ required. These circuits are the compiled versions of those in Fig. 17 for use on IBM's QPU.

3. Standard VQE quantum circuits

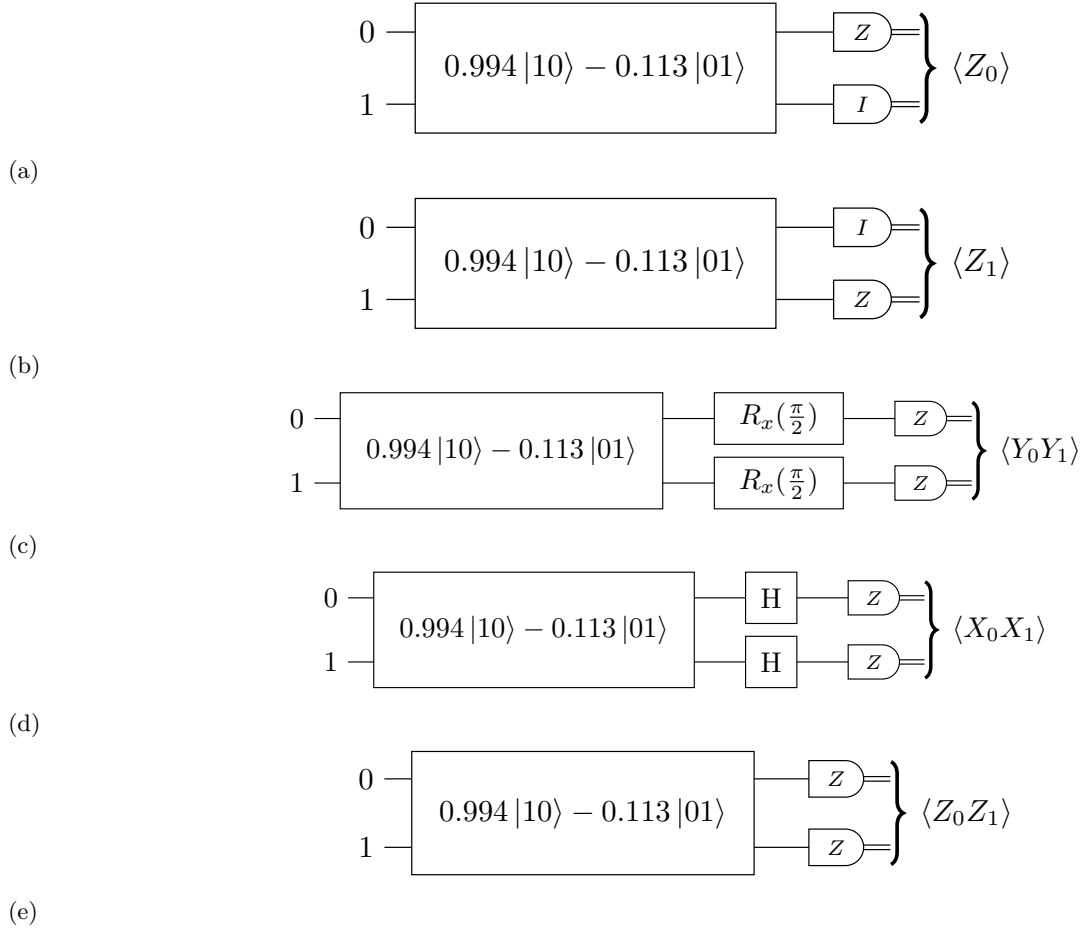


FIG. 19: Quantum circuits required to find the ground state of H_2 using standard VQE. Each operator in Table I requires a separate measurement.

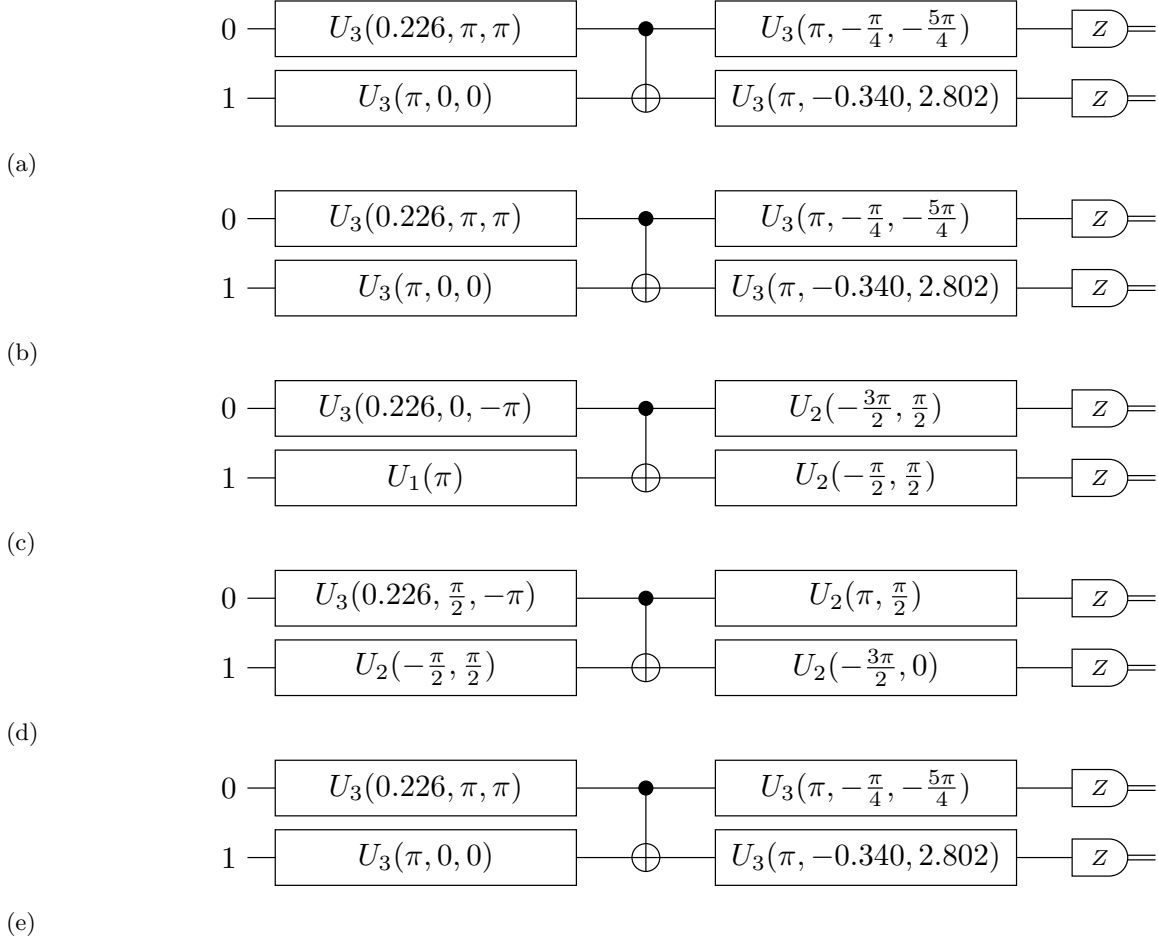


FIG. 20: Quantum circuits required to find the ground state of H_2 using standard VQE. These circuits are the compiled versions of those in Fig. 19 for use on IBM's QPU.

4. Measurement error mitigation

The measurement error mitigation strategy employed in our work was a simple inversion procedure [55] available in qiskit. The quantum circuits required were generated by the qiskit.ignis *complete_meas_cal* method and executed alongside each separate ibmqx2 experiment, with the maximum number of shots (8192). This sampling cost was not included in the fixed number of calls to quantum device. The *CompleteMeasFitter* method in qiskit.ignis [33] was used to generate the calibration matrix required for measurement error mitigation [33, 55].

B. Lithium Hydride

In the STO-6G basis the qubit Hamiltonian for LiH contains 631 terms. We considered a bond length of $R(\text{Li-H})=1.45 \text{ \AA}$. In total there are 12 spin-orbitals and the number of qubits required to simulate this system with no reductions is 12. This has been included as an XLS file.

The same method given in Section III A was used to partition the Hamiltonian into anticommuting sets and 102 cliques were obtained. They have been included in the XLS file. The operators used to implement the sequence of rotations and LCU methods have also been included in this file.

The first sheet of the XLS document contains the LiH Hamiltonian. The first column contains each c_i coefficient and the second column the associated P_i term. In total 631 rows. Note that P_i operators written as $[]$ represent the n -fold identity operation.

The second sheet contains the the anticommuting sets H_{S_i} . It has the same structure as Table I and contains 102 sets.

The third sheet gives the operators required to perform unitary partitioning via a sequence of rotations, given the clique cover from the first sheet. It follows the same structure as Table II and contains 98 entries.

The final sheet gives the operators required to perform unitary partitioning via a LCU, given the clique cover from the first sheet. It follows the same structure as Table III and contains 98 entries.

Due to the size of each quantum circuit, they were each simulated once using qiskit's *statevector_simulator* and the final statevectors obtained were sampled from using qiskit's Statevector class *sample_counts* method [33]. This gives qubit measurement outcomes in the computational basis. In our simulation, each control P_i gate required by the LCU method was directly simulated, and neither work qubits nor circuit simplifications were used.

C. Statistical analysis

Molecule	Method	Backend	N	$\langle E \rangle / Ha$	$\langle E \rangle$ 95%CI / Ha	σ_{e_j} / Ha	σ_{e_j} 95%CI / Ha	SEM / Ha	SEM 95%CI / Ha
H2	LCU	ibmqx2 - mit	332763	-1.0212	[-1.0222, -1.0201]	3.1661e-01	[3.1504e-01, 3.1816e-01]	5.4886e-04	[5.4617e-04, 5.5158e-04]
H2	SeqRot	ibmqx2 - mit	421951	-1.0246	[-1.0256, -1.0237]	3.1984e-01	[3.1838e-01, 3.2132e-01]	4.9239e-04	[4.9017e-04, 4.9459e-04]
H2	standard	ibmqx2 - mit	253074	-1.0381	[-1.0394, -1.0367]	3.4240e-01	[3.4053e-01, 3.4424e-01]	6.8063e-04	[6.7697e-04, 6.8432e-04]
H2	LCU	ibmqx2 - raw	333407	-0.54537	[-0.54757, -0.54315]	6.5287e-01	[6.5129e-01, 6.5442e-01]	1.1307e-03	[1.1279e-03, 1.1334e-03]
H2	SeqRot	ibmqx2 - raw	422100	-0.55863	[-0.56063, -0.55666]	6.5025e-01	[6.4885e-01, 6.5162e-01]	1.0009e-03	[9.9873e-04, 1.0030e-03]
H2	standard	ibmqx2 - raw	253260	-0.76468	[-0.76685, -0.76247]	5.6625e-01	[5.6441e-01, 5.6810e-01]	1.1252e-03	[1.1215e-03, 1.1287e-03]
H2	LCU	simulator	336390	-1.1373	[-1.1374, -1.1373]	1.5655e-02	[1.4307e-02, 1.7082e-02]	2.6992e-05	[2.4692e-05, 2.9392e-05]
H2	SeqRot	simulator	422100	-1.1373	[-1.1373, -1.1372]	1.6286e-02	[1.5084e-02, 1.7533e-02]	2.5068e-05	[2.3147e-05, 2.6968e-05]
H2	standard	simulator	253260	-1.1370	[-1.1377, -1.1363]	1.7752e-01	[1.7634e-01, 1.7872e-01]	3.5276e-04	[3.5040e-04, 3.5512e-04]
LiH	LCU	simulator	1447349	-7.9719	[-7.9723, -7.9714]	2.7268e-01	[2.7213e-01, 2.7322e-01]	2.2665e-04	[2.2620e-04, 2.2711e-04]
LiH	SeqRot	simulator	9985500	-7.9712	[-7.9714, -7.9710]	2.7292e-01	[2.7271e-01, 2.7312e-01]	8.6367e-05	[8.6303e-05, 8.6432e-05]
LiH	standard	simulator	1616700	-7.9716	[-7.9720, -7.9712]	2.6817e-01	[2.6773e-01, 2.6860e-01]	2.1091e-04	[2.1056e-04, 2.1125e-04]

TABLE IV: The mean, standard deviation and standard error on the mean for each method calculating the ground state energies of H_2 and LiH using single-shot VQE. The simulator backend represents a noise-free QPU emulator and ibmqx2 a real quantum device. Ibmqx2-raw are the raw experimental results from the QPU and ibmqx2-mit with measurement error mitigation applied. 95% confidence intervals (CI) were calculated using bootstrap resampling [36].

D. LiH histogram results

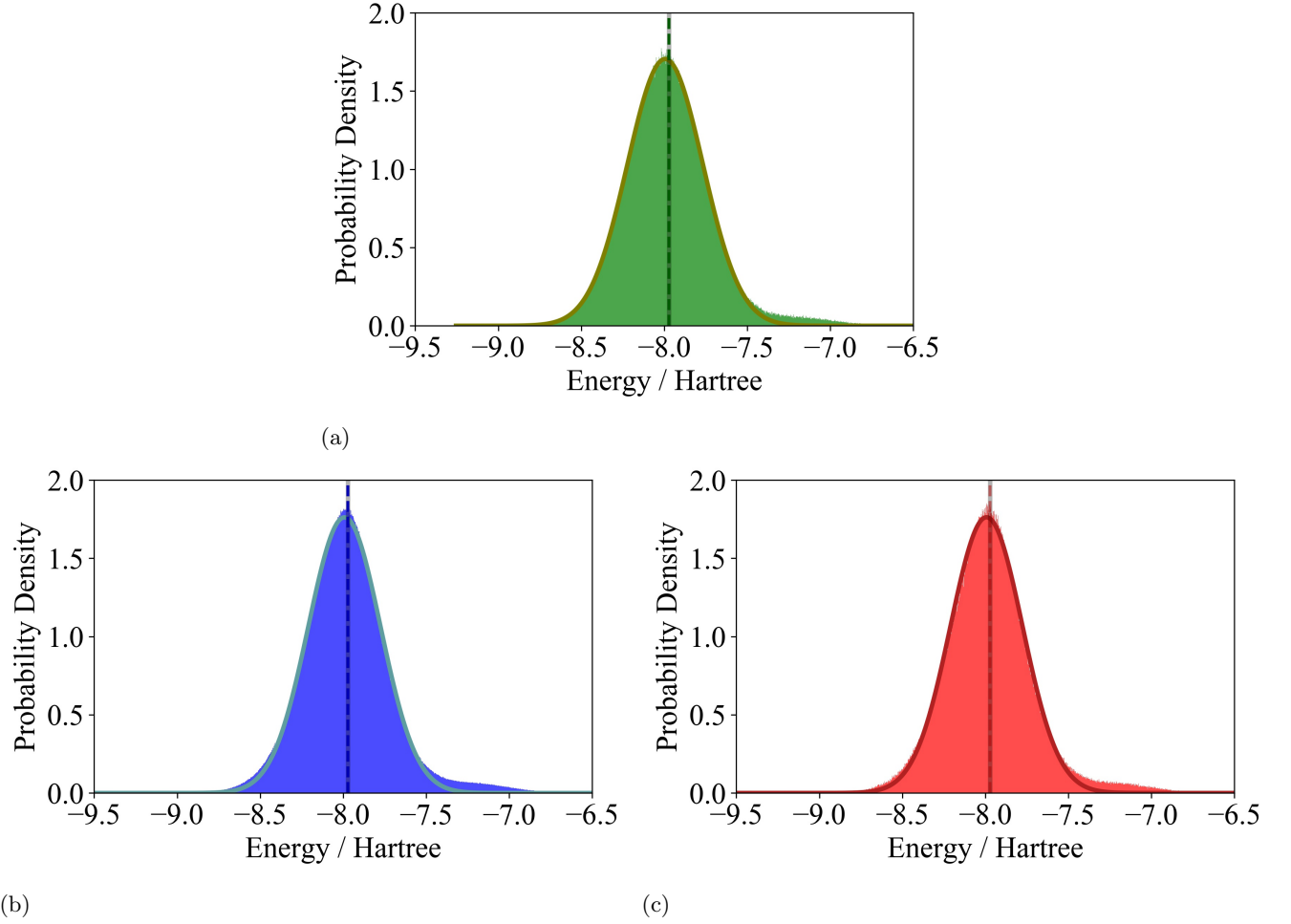


FIG. 21: Probability density function of different single-shot VQE calculations used to estimate the ground state energy e_j of LiH. All results here are from a noise-free QPU emulation. The green results (a) are data from standard VQE. The blue (b) and red (c) data are results from VQE with unitary partitioning applied as a sequence of rotations and a LCU respectively. The number of bins was set to 2500 for all histograms and a Gaussian was fitted to each result. The dashed vertical lines show the average energy for each method and each solid black vertical line shows the FCI ground state energy ($-7.97118 Ha$).